

**M.Tech**

**(Computational Design)**

**[Saurabh Bhardwaj]**

**2018**

**BONDGRAPH ANALYSIS OF DYNAMIC  
INTERACTION BETWEEN THE CONCRETE SLAB  
AND SUBGRADE FOR HIGH SPEED TRACK**

A THESIS SUBMITTED IN PARTIAL FULFILLMENT OF THE  
REQUIREMENT FOR THE DEGREE OF

**MASTER OF TECHNOLOGY**

IN

**COMPUTATIONAL DESIGN (CDN)**

SUBMITTED BY

**SAURABH BHARDWAJ**

(2K17/CDN/04)

UNDER THE SUPERVISION OF

**PROF. VIKAS RASTOGI**

PROFESSOR



DEPARTMENT OF MECHANICAL ENGINEERING

DELHI TECHNOLOGICAL UNIVERSITY

(Formerly Delhi College of Engineering)

Shahbad Daulatpur, Main Bawana Road, Delhi-110042

JUNE 2019

## **STUDENT'S DECLARATION**

I, Saurabh Bhardwaj, Roll No(s). 2k17/CDN/04 student of M.Tech (Computational Design), hereby declare that the thesis entitled "**BONDGRAPH ANALYSIS OF DYNAMIC INTERACTION BETWEEN THE CONCRETE SLAB AND SUBGRADE FOR HIGH SPEED TRACK**" which is submitted by me to the Department of Mechanical Engineering, Delhi Technological university, Delhi in partial fulfillment of the requirement for the award of the degree of Master Of Technology, is original and not copied from any source without proper citation. This work has not previously formed the basis for the award of any Degree, Diploma Associateship, Fellowship or other similar title or recognition.

Place: Delhi

Date:

Saurabh Bhardwaj

2K17/CDN/04

## **CERTIFICATE**

I hereby certify that the Dissertation entitled "**Bond graph analysis of Dynamic Interaction between the Concrete slab and Subgrade for High Speed Track**" which is submitted by Saurabh Bhardwaj, Roll No. 2k17/CDN/04 Mechanical Engineering Department, Delhi Technological University, Delhi in partial fulfillment of the requirement for the award of the degree Of Master of Technology, is a record of the project work carried out by the students under my supervision. To the best of my knowledge this work has not been submitted in part or full for any Degree or Diploma to this University or elsewhere.

Prof. Vikas Rastogi  
Professor  
(Project Mentor)

## **ACKNOWLEDGEMENT**

Research is a higher concept. It brings to test our patience, vigour, and dedication. Every result arrived is a beginning for a higher achievement. My project is a small drop in an ocean. It needs the help of friends and guidance of experts in the field, to achieve something new.

I found my pen incompetent to express my thanks to my guide and **mentor Prof. Vikas Rastogi, Professor, DTU** under whose kind and worthy guidance and supervision, I had the opportunity to carry out this work. It was only due to his advice, thoughtful comments, constructive criticism, and continuous vigil over the progress of my work with a personal interest that it has taken this shape. They have been a great source of encouragement.

To get an opportunity to carry out the project work in the well-equipped, ever developing laboratories in our institution, I would like to pay my deep sense of thankfulness to **Prof. Vipin, HOD, Department of Mechanical Engineering, DTU**.

I am especially thankful to **Ms. Yamika Patel, Ph.D. Scholar, DTU** as I have completed my project under her worthy guidance and supervision. Her advice and thoughtful comments inspired me and were very helpful to complete my project.

I am very much thankful to my parents for their moral support and encouragement, which was giving me the strength to chase my goal. Without their support and inspiration, I would not be able to complete my degree.

I would especially like to acknowledge my gratitude to all my dear friends for their consistent support, valuable suggestions from time to time to make this project worthy.

I take this opportunity to express my gratitude to all those who have supported me in completing my fourth-semester project work as a part of my degree program.

**SAURABH BHARDWAJ**

**M. Tech (Computational Design)**

**2K17/CDN/04**

## **ABSTRACT**

In the last few years there has been a major shift from petrol, diesel vehicles to electric vehicles and other alternate fuel vehicles, because of the limited availability of fossil fuels. High speed train is one such example of electric vehicles, that have witnessed an increasing demand in present times, specially in urban cities, due to its various advantages, namely, ease of use, economical, time saving, and comfortable. As a result of these factors, analysis and study of such systems, for their optimal performance and more economical operation, is of paramount concern.

The present-day study is aimed to elucidate the effect of vehicle speed on the deflection between the concrete slab/subgrade contact, and track components. The interaction between the slab and the subgrade, affects the safety and comfort of the vehicle. The dynamic analysis of a three-dimensional, modal Bond graph model of the high-speed track components is carried out in this article. The concrete slab is modelled as a Euler-Bernoulli beam, and the beam is divided into 5 nodes. Two parallel slabs are joined with cement-asphalt mortar between them. The hence developed model is then simulated for train velocities ranging from 200kmph to 500kmph. The bond graph modelling and its simulation, is performed using SYMBOLS SHAKTI software.

# CONTENTS

STUDENT'S DECLARATION	ii
CERTIFICATE	iii
ACKNOWLEDGEMENT	iv
ABSTRACT	v
CONTENTS	vi
LIST OF FIGURES	ix
LIST OF TABLES	xv
LIST OF NOMENCLATURE	xv
<b>CHAPTER 1. INTRODUCTION</b>	<b>1</b>
1.1 High Speed Railway track versus Conventional Railway track	1
1.2 Modelling of High-speed railway track	2
1.3 Bond Graph	4
1.3.1 Components of Bond Graph	5
1.3.2 Causality	10
1.4 Research Objectives	12
1.5 Organisation of Thesis	13
<b>CHAPTER 2. LITERATURE REVIEW</b>	<b>14</b>
<b>CHAPTER 3. COMPUTATIONAL MODELS OF HIGH-SPEED TRACK AND METHODOLOGY</b>	<b>20</b>
3.1 Numerical Modelling	20
3.2 Bond Graph Modelling	23
3.3 Methodology	26

<b>CHAPTER 4. SIMULATION STUDY</b>	<b>27</b>
4.1 Case I – Deflection in Concrete Slab	30
4.1.1 Mode – 1	30
4.1.2 Mode – 2	31
4.1.3 Mode – 3	32
4.1.4 Mode – 4	33
4.1.5 Mode – 5	34
4.2 Case II – Deflection in Subgrade	35
4.2.1 Mode – 1	35
4.2.2 Mode – 2	36
4.2.3 Mode – 3	37
4.2.4 Mode – 4	38
4.2.5 Mode – 5	39
4.3 Case III – Lateral Deflection between Concrete Slabs	40
4.3.1 Mode – 1	40
4.3.2 Mode – 2	41
4.3.3 Mode – 3	42
4.3.4 Mode – 4	43
4.3.5 Mode – 5	44
4.4 Case IV – Fast Fourier Transform (FFT) for concrete slab	45
4.4.1 Mode – 1	45
4.4.2 Mode – 2	45
4.4.3 Mode – 3	46
4.4.4 Mode – 4	46
4.4.5 Mode – 5	47
4.5.6 Velocity 200 kmph	48
4.5.7 Velocity 300 kmph	48
4.5.8 Velocity 400 kmph	49

4.5.9 Velocity 500 kmph	49
<b>CHAPTER 5. CONCLUSION AND RESULTS</b>	<b>51</b>
REFERENCES	52
APPENDIX	54



## LIST OF FIGURES

<b>Figure No.</b>	<b>Figure Name</b>	<b>Page No.</b>
1.1	High speed train/track model with ballasted track	3
1.2	A cross section view of two-dimensional model of slab track	4
1.3	Bond representation for source (effort and flow) element	5
1.4	Bond representation for sink (effort and flow) element	5
1.5	Bond representation for inertance element	6
1.6	Bond representation for resistance element	6
1.7	Bond representation for capacitance element	6
1.8	Bond representation for transformer element	7
1.9	Bond representation for gyrator element	7
1.10	Bond representation for 0-junction element	8
1.11	Bond representation for 1-junction element	9
1.12	Concept of causality with Source of Effort element	10
1.13	Concept of causality with Inertance and Capacitance element	10
1.14	Concept of causality with Resistance element	11
1.15	Concept of causality with Transformer element	11
1.16	Concept of causality with Gyrator element	12
3.1	Concrete Slab - Sub grade model, connected with spring damper system	20
3.2	Bond graph model of the concrete slab and sub grade system	23
3.3	Three-dimensional Bond graph modal model of the concrete slab and sub-grade system, subjected to a constant moving load	25
4.1	Deflection (m) vs Time (s) graph for Mode 1 of Concrete Slab at 200 kmph	30

4.2	Deflection (m) vs Time (s) graph for Mode 1 of Concrete Slab at 300 kmph	30
4.3	Deflection (m) vs Time (s) graph for Mode 1 of Concrete Slab at 400 kmph	30
4.4	Deflection (m) vs Time (s) graph for Mode 1 of Concrete Slab at 500 kmph	30
4.5	Deflection (m) vs Time (s) graph for Mode 2 of Concrete Slab at 200 kmph	31
4.6	Deflection (m) vs Time (s) graph for Mode 2 of Concrete Slab at 300 kmph	31
4.7	Deflection (m) vs Time (s) graph for Mode 2 of Concrete Slab at 400 kmph	31
4.8	Deflection (m) vs Time (s) graph for Mode 2 of Concrete Slab at 500 kmph	31
4.9	Deflection (m) vs Time (s) graph for Mode 3 of Concrete Slab at 200 kmph	32
4.10	Deflection (m) vs Time (s) graph for Mode 3 of Concrete Slab at 300 kmph	32
4.11	Deflection (m) vs Time (s) graph for Mode 3 of Concrete Slab at 400 kmph	32
4.12	Deflection (m) vs Time (s) graph for Mode 3 of Concrete Slab at 500 kmph	32
4.13	Deflection (m) vs Time (s) graph for Mode 4 of Concrete Slab at 200 kmph	33
4.14	Deflection (m) vs Time (s) graph for Mode 4 of Concrete Slab at 300 kmph	33
4.15	Deflection (m) vs Time (s) graph for Mode 4 of Concrete Slab at 400 kmph	33

4.16	Deflection (m) vs Time (s) graph for Mode 4 of Concrete Slab at 500 kmph	33
4.17	Deflection (m) vs Time (s) graph for Mode 5 of Concrete Slab at 200 kmph	34
4.18	Deflection (m) vs Time (s) graph for Mode 5 of Concrete Slab at 300 kmph	34
4.19	Deflection (m) vs Time (s) graph for Mode 5 of Concrete Slab at 400 kmph	34
4.20	Deflection (m) vs Time (s) graph for Mode 5 of Concrete Slab at 500 kmph	34
4.21	Deflection (m) vs Time (s) graph for Mode 1 of Sub grade at 200 kmph	35
4.22	Deflection (m) vs Time (s) graph for Mode 1 of Sub grade at 300 kmph	35
4.23	Deflection (m) vs Time (s) graph for Mode 1 of Sub grade at 400 kmph	35
4.24	Deflection (m) vs Time (s) graph for Mode 1 of Sub grade at 500 kmph	35
4.25	Deflection (m) vs Time (s) graph for Mode 2 of Sub grade at 200 kmph	36
4.26	Deflection (m) vs Time (s) graph for Mode 2 of Sub grade at 300 kmph	36
4.27	Deflection (m) vs Time (s) graph for Mode 2 of Sub grade at 400 kmph	36
4.28	Deflection (m) vs Time (s) graph for Mode 2 of Sub grade at 500 kmph	36
4.29	Deflection (m) vs Time (s) graph for Mode 3 of Sub grade at 200 kmph	37

4.30	Deflection (m) vs Time (s) graph for Mode 3 of Sub grade at 300 kmph	37
4.31	Deflection (m) vs Time (s) graph for Mode 3 of Sub grade at 400 kmph	37
4.32	Deflection (m) vs Time (s) graph for Mode 3 of Sub grade at 500 kmph	37
4.33	Deflection (m) vs Time (s) graph for Mode 4 of Sub grade at 200 kmph	38
4.34	Deflection (m) vs Time (s) graph for Mode 4 of Sub grade at 300 kmph	38
4.35	Deflection (m) vs Time (s) graph for Mode 4 of Sub grade at 400 kmph	38
4.36	Deflection (m) vs Time (s) graph for Mode 4 of Sub grade at 500 kmph	38
4.37	Deflection (m) vs Time (s) graph for Mode 5 of Sub grade at 200 kmph	39
4.38	Deflection (m) vs Time (s) graph for Mode 5 of Sub grade at 300 kmph	39
4.39	Deflection (m) vs Time (s) graph for Mode 5 of Sub grade at 400 kmph	39
4.40	Deflection (m) vs Time (s) graph for Mode 5 of Sub grade at 500 kmph	39
4.41	Deflection (m) vs Time (s) graph for Mode 1 of Concrete Slab at 200 kmph	40
4.42	Deflection (m) vs Time (s) graph for Mode 1 of Concrete Slab at 300 kmph	40
4.43	Deflection (m) vs Time (s) graph for Mode 1 of Concrete Slab at 400 kmph	40

4.44	Deflection (m) vs Time (s) graph for Mode 1 of Concrete Slab at 500 kmph	40
4.45	Deflection (m) vs Time (s) graph for Mode 2 of Concrete Slab at 200 kmph	41
4.46	Deflection (m) vs Time (s) graph for Mode 2 of Concrete Slab at 300 kmph	41
4.47	Deflection (m) vs Time (s) graph for Mode 2 of Concrete Slab at 400 kmph	41
4.48	Deflection (m) vs Time (s) graph for Mode 2 of Concrete Slab at 500 kmph	41
4.49	Deflection (m) vs Time (s) graph for Mode 3 of Concrete Slab at 200 kmph	42
4.50	Deflection (m) vs Time (s) graph for Mode 3 of Concrete Slab at 300 kmph	42
4.51	Deflection (m) vs Time (s) graph for Mode 3 of Concrete Slab at 400 kmph	42
4.52	Deflection (m) vs Time (s) graph for Mode 3 of Concrete Slab at 500 kmph	42
4.53	Deflection (m) vs Time (s) graph for Mode 4 of Concrete Slab at 200 kmph	43
4.54	Deflection (m) vs Time (s) graph for Mode 4 of Concrete Slab at 300 kmph	43
4.55	Deflection (m) vs Time (s) graph for Mode 4 of Concrete Slab at 400 kmph	43
4.56	Deflection (m) vs Time (s) graph for Mode 4 of Concrete Slab at 500 kmph	43
4.57	Deflection (m) vs Time (s) graph for Mode 5 of Concrete Slab at 200 kmph	44

4.58	Deflection (m) vs Time (s) graph for Mode 5 of Concrete Slab at 300 kmph	44
4.59	Deflection (m) vs Time (s) graph for Mode 5 of Concrete Slab at 400 kmph	44
4.60	Deflection (m) vs Time (s) graph for Mode 5 of Concrete Slab at 500 kmph	44
4.61	Deflection (m) vs Frequency (Hz) Fast Fourier Transform curve of Mode 1 of Concrete Slab at different velocities	45
4.62	Deflection (m) vs Frequency (Hz) Fast Fourier Transform curve of Mode 2 of Concrete Slab at different velocities	45
4.63	Deflection (m) vs Frequency (Hz) Fast Fourier Transform curve of Mode 3 of Concrete Slab at different velocities	46
4.64	Deflection (m) vs Frequency (Hz) Fast Fourier Transform curve of Mode 4 of Concrete Slab at different velocities	46
4.65	Deflection (m) vs Frequency (Hz) Fast Fourier Transform curve of Mode 5 of Concrete Slab at different velocities	47
4.66	Deflection (m) vs Frequency (Hz) Fast Fourier Transform curve of different modes of Concrete Slab at 200 kmph velocities	48
4.67	Deflection (m) vs Frequency (Hz) Fast Fourier Transform curve of different modes of Concrete Slab at 200 kmph velocities	48
4.68	Deflection (m) vs Frequency (Hz) Fast Fourier Transform curve of different modes of Concrete Slab at 200 kmph velocities	48
4.69	Deflection (m) vs Frequency (Hz) Fast Fourier Transform curve of different modes of Concrete Slab at 200 kmph velocities	48

## LIST OF TABLES

<b>Table No.</b>	<b>Name of Table</b>	<b>Page No.</b>
1.1	High Speed Railway Track vs Conventional Railway Track	2
4.1	Material properties of the components of high-speed track	28

## LIST OF NOMENCLATURE

BG	Bondgraph
I	Inertance
C	Capacitance
R	Resistance
SE	Source of effort
SF	Source of flow
TF	Transformer
GY	Gyrator
Q	Displacement
P	Momentum
t	Time

# CHAPTER 1

## INTRODUCTION

The railway train running along a track comprises of various degrees of freedoms as it comprises of many parts. It is one of the most complicated dynamic systems in engineering, and the most important mode of public transport in a country like India where it runs more than 20,000 passenger trains daily. Indian Railways are the fourth largest railway network in the world, that consists of 69,128-kilometre route, as of April 2019

A moving interface connects the vehicle with the track. The vehicle and the track, together, form the railway system and it usually comprises of a car body, bogie, primary and secondary suspensions, wheelsets, track, sleepers/concrete slabs, ballast, and subgrade.

All over the world, the railway industries are making considerable efforts to increase the speeds and load carrying capacity of trains. In India, the average speed of freight trains is around 24 kmph, and the express trains, the most common types, run at an average speed of 50.6 kmph. Constant efforts are being made in the direction to increase the speed of trains, and also to introduce high speed trains, alongside the conventional ones. However, there is a trade-off between increased train speed and load carrying capacity, and the vibrations produced in the vehicle-track system due to wheel/rail irregular surface, which, then further raises the possibility of damage to the track component. The safe running of the train, and rider comfort are adversely affected by this. Also, the nonlinear relationship between wheel/rail contact and the track components make the system more complex. Thus, significant efforts have been needed for reliable predictions of wheel/rail interaction forces to get the key factors responsible for damage of vehicle and track components.

### **1.1 High Speed Railway track versus Conventional Railway track:**

High speed tracks are more complicated than conventional track systems. Smaller track gauge and larger cant deficiency are some of the characteristic features of high-speed railway systems. A list of differences in the track design standards of conventional and high-speed railways are given below in Table -:



	<b>High Speed Railway track (Common European Standard), Mixed Traffic</b>	<b>Conventional Railway Track (Indian Railway), Mixed Traffic</b>
<b>Track Gauge</b>	1435mm (Standard Gauge)	1676 mm (Broad Gauge)
<b>Train Length</b>	400m	
<b>Speed</b>	<230 kmph	<160 kmph
<b>Cant <math>C_a</math></b>	160 mm	165 mm
<b>Cant deficiency <math>C_d</math></b>	140	100
<b>Cant excess <math>C_e</math></b>	110 mm	75 mm
<b>Gradient</b>	10% (Sweden) 12.5% (Germany)	10%
<b>Radius (min), V-Curve</b>		4000 m

**Table 1.1:** High Speed Railway Track vs Conventional Railway Track

High-speed trains have been growing as a popular mode of public transportation, since the time it has been constructed and brought into operation. This is due to the drastic advantages in the departments of speed, accessibility, green-design, comfortability, increased capacity, low power, unaffected by the weather, etc. According to the statistics from the International Union of railways (UIC), up to November 1, 2013, the total operation mileage of the high-speed railways of other countries and regions in the world is 11605 km. 4883-km high-speed railways are under construction, and 12570-km high-speed railways are planned to be constructed.

## **1.2 Modelling of High-speed railway track:**

Railroad technology, since the first train track, that used wooden sleepers, has been evolving and growing, for approximately 150 years. For most of this duration, ballasted track system which was the conventional track system, has consisted of certain components including rails, ties, ballast, and the subgrade (roadbed). A conventional ballasted railway track model is shown in Figure 1.

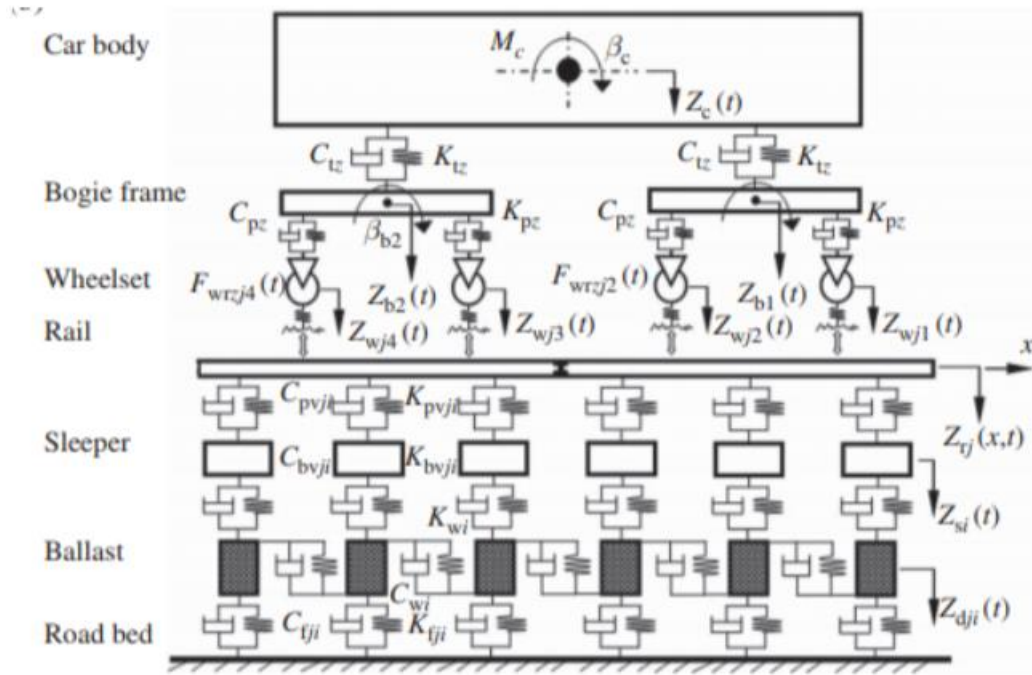


**Fig.1.1:** High speed train/track model with ballasted track

With increasing speeds of trains with time, a more reliable, durable and stable track system is required in place. Ballast-less track proves to be a solution of this problem. There has been an increase in the use of concrete slab technology over the last 20 years, for high-speed train applications. The non-ballasted track is made of steel rail, railway fasteners and slab. The concrete slab, in place of the ballast, proves to be a more stable alternative for the higher speeds of operation that are desired in high speed trains. Ballasted tracks are cheaper as compared to the concrete slab tracks, but it makes up for the high cost with lesser maintenance and a higher serviceability with a longer operational life. Therefore, in the longer run, the concrete slab proves to be a better alternative to the ballasted track in all aspects.

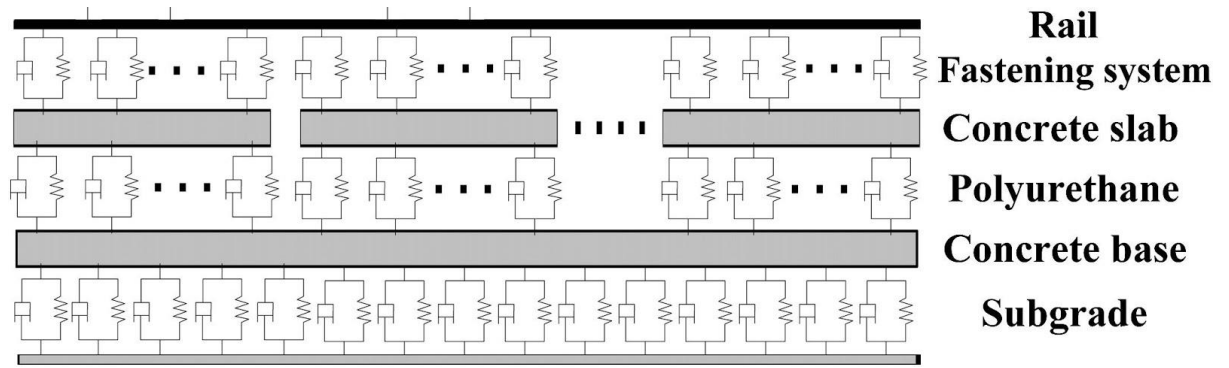


**Fig.1.2:** A cross section view of two-dimensional model of slab track

In Figure 2, a two-dimensional model of the slab track interaction is shown. The track constitutes of three layers, namely, the rail in form of a continuous layer, followed by the discontinuous concrete slab, and in the end, the concrete base, which is considered as a continuous layer, is modelled accordingly. The third layer has several sub-parts. A similar track, connected by a common concrete base, runs parallel to the track shown in the 2-D model. A common three-dimensional model of the track becomes complex in itself and has a lot of components.

With longer running time at high speeds, the track deflections and vibrations at the sub grade level increase accordingly. This is detrimental to the train running quality, and poses threat of damage to other parts of the system as well. The lateral forces and deflections come into picture due to traction and braking, and affect the operation of the whole system in a complex manner. This in turn causes derailment, hunting, and affect the ride comfort. Therefore, the study of deflections at the sub grade level, and laterally between the common concrete slabs is the basis of investigation in this paper.

### 1.3 Bond Graph

Bond graphs are a domain-independent graphical description of dynamic behaviour of physical systems. This means that systems from different domains (cf. electrical, mechanical, hydraulic, acoustical, thermodynamic, material) are described in the same way. The basis is that bond graphs are based on energy and energy exchange. Analogies between domains are more than just equations being analogous: the used physical concepts are analogous. [5] It is an explicit graphical tool for capturing the common energy structure of systems. It increases one's insight into systems behaviour. In the vector form, they give concise description of complex systems.

Moreover, the notations of causality provide a tool not only for formulation of system equations, but also for intuition-based discussion of system behaviour, viz. controllability, observability, fault diagnosis, etc. [9]

### 1.3.1 Components of Bond Graph

#### Single-port elements

The elements with one port are called single-port elements.

**Sources and sinks:** The elements that denote the input for the system are called source. Their job is to input flow or effort in the system. Their representation is done as  $S_e$  and  $S_f$  for Source of Flow and Source of Effort, respectively. Sinks have an arrow pointing towards them, whereas the sources have them pointing in their direction. Example of a source: motors (source of effort,  $S_e$  torque), voltage sources (source of effort,  $S_e$ ), and current sources (source of flow,  $S_f$ ).

$$S_e \longrightarrow J \quad \text{and} \quad S_f \longrightarrow J$$

**Fig.1.3:** Bond representation for source (effort and flow) element

The elements that denote the output for the system are called sinks. Their representation is done in a similar fashion as that of the source, the only difference being, they have the arrow pointing away from them .

$$J \longrightarrow S_e \quad \text{and} \quad J \longrightarrow S_f$$

**Fig.1.4:** Bond representation for sink (effort and flow) element

**Inertance:** The elements that denoted by the symbol “I”, represent Inertance. The direction of power flow is always towards Inertance element. Kinetic energy is stored in these elements. The most common representation of these elements is in the form of masses, when talking in terms of mechanical component, and in the form of inductance, when talking about the electrical components.

$$J \longrightarrow I$$

**Fig.1.5:** Bond representation for inertance element

**Resistance:** The elements that denoted by the symbol “R”, represent Resistance. The direction of power flow is always towards Resistance element. Energy is dissipated out of these elements. The most common representation of these elements is in the form of dampener, when talking in terms of mechanical component, and in the form of resistors, when talking about the electrical components.

$$J \longrightarrow R$$

**Fig.1.6:** Bond representation for resistance element

**Capacitance:** The elements that denoted by the symbol “C”, represent Capacitance. The direction of power flow is always towards Capacitance element. Potential energy is stored in these elements. The most common representation of these elements is in the form of springs, when talking in terms of mechanical component, and in the form of capacitors, when talking about the electrical components.

$$J \longrightarrow C$$

**Fig.1.7:** Bond representation for capacitance element

### **Two-port elements**

The elements that have two ports are called Two-port elements. They function as the conveyer of power between the system. When the conversion of power takes place through these elements, there is no loss in transfer. The elements come along with a constant of their own. Depending on the element that is being used the constant is either a transformer constant or a gyrator constant. The most common representation of these constants is in the form of a ratio of the elements.

**Transformer:** Transformer is a type of two port element which defines a relationship between flow-in and flow-out, or effort-in and effort-out, depending on the type of elements. Examples of a transformer include, an electric transformer, or a mechanical lever, denoted as -

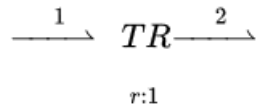


**Fig.1.8:** Bond representation for transformer element

where the  $r$  denotes the modulus of the transformer. This means

$$f_1 \cdot r = f_2 \tag{1.1}$$

and

$$e_2 \cdot r = e_1 \tag{1.2}$$

**Gyrator:** Gyrator is a type of two port element which defines a relationship between flow-in and effort-out, or effort-in and flow-out, depending on the type of element. Examples of a gyrator include, a DC motor, which converts voltage (electrical effort) into Angular velocity (angular mechanical flow).

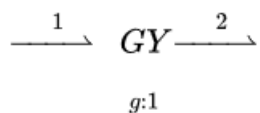


**Fig.1.9:** Bond representation for gyrator element

meaning that

$$e_2 = g \cdot f_1 \tag{1.3}$$

and

$$e_1 = g \cdot f_2. \tag{1.4}$$

### Multi-port elements

The Junctions, in which there is no restriction upon the number of ports, like the elements mentioned above, are called multi-port elements. Junctions divide the power across all their ports. Depending upon the way the elements carry out the effort and flow, they are divided into 1-junction and 0-junction. When the same junctions are in series, they can be combined, but different junctions in series cannot be combined.

**0-junctions:** When a 0-junction is connected in a bond graph model, the effort values, across all the bonds, connected to the 0-element, are equal, and the sum of all the flow values into the element, is equal to sum of flow values out of the element.

*all e' s are equal*

$$\sum f_{in} = \sum f_{out}$$

(1.5)

An example is shown below.

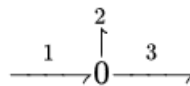


**Fig.1.10:** Bond representation for 0-junction element

Resulting equations:

$$e_1 = e_2 = e_3 \tag{1.6}$$

$$f_1 = f_2 + f_3 \tag{1.7}$$

**1-junctions:** The behaviour of 1-junctions is exactly opposite to that of a 0-junction. When a 1-junction is connected in a bond graph model, the flow values, across all the bonds, connected to the 1-element, are equal, and the sum of all the effort values into the element, is equal to sum of effort values out of the element.

*all f' s are equal*

$$\sum e_{in} = \sum e_{out} \tag{1.8}$$

An example is shown below.

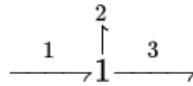


**Fig.1.11:** Bond representation for 1-junction element

Resulting equations:

$$f_1 = f_2 = f_3 \tag{1.9}$$

$$e_1 = e_2 + e_3 \tag{1.10}$$



### 1.3.2 Causality

In terms of Bond graphs, Causality determines the assignment of instantaneous effort and instantaneous flow, to the side, or ends of the bond. The dependence or the independence of a variable is determined by the causality, for every modelling element, while the formulation of dynamic equations which define the system, takes place. The ease of analysis of a large model, increases by moving the causality from one element to other. When the bond graph is correctly causal, the algebraic loop where a variable is a recursive function of itself, can easily be detected. Causality is a symmetric relationship, where one side "causes" effort, the other side "causes" flow.

When assigning causality to a bond graph model, the causal stroke is added to one end of the bond (power bond), which implies that the other end is for effort. Consider a constant-torque motor driving a wheel, i.e. a source of effort (*SE*). That would be drawn as follows:

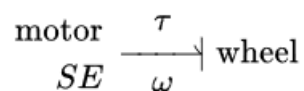


**Fig.1.12:** Concept of causality with Source of Effort element

Similarly the side of the power bond with the causal stroke at the end denotes the flow for the bond.

Compatibility constraints are the outcome of Causation in a bond graph model. Effort and causal strokes can only be at the opposite ends of a power bond. Also, *I* and *C*, which are the two passive components having time-dependent behaviour, can only have one sort of causation: an *I* component illustrates flow; a *C* component denominates effort. So, from a junction, *J*, the preferred causal orientation is as follows:

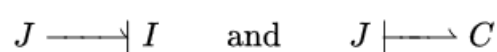


**Fig.1.13:** Concept of causality with Inertance and Capacitance element

It is the preferred method because these elements can be further analysed if these equations are considered

$$f(t) = \frac{1}{I} \int e(t) dt \quad \text{and} \quad e(t) = \frac{1}{C} \int f(t) dt$$

The equations that are obtained prefer the results of causality, as a result of independent power variable integral instead of the derivative results. The equations can be seen below.

$$e(t) = I \cdot \dot{f}(t) \quad \text{and} \quad f(t) = C \cdot \dot{e}(t)$$

It is possible for a bond graph to have a casual bar on one of these elements in the non-preferred manner. In such a case a "casual conflict" is said to have occurred at that bond. The results of a casual conflict are only seen when writing the state-space equations for the graph. It is explained in more details in that section.

A resistor has no time-dependent behaviour: apply a voltage and get a flow instantly, or apply a flow and get a voltage instantly, thus a resistor can be at either end of a causal bond:

$$J \text{ ---| } R \quad \text{and} \quad J \text{ |--- } R$$

**Fig.1.14:** Concept of causality with Resistance element

Sources of flow (*SF*) define flow, sources of effort (*SE*) define effort. Transformers are passive, neither dissipating nor storing energy, so causality passes through them:

$$\text{---| } TF \text{ ---|} \quad \text{or} \quad \text{|--- } TF \text{ |---}$$

**Fig.1.15:** Concept of causality with Transformer element

A gyrator transforms flow to effort and effort to flow, so if flow is caused on one side, effort is caused on the other side and vice versa:

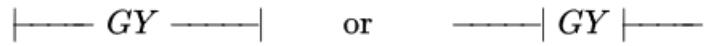
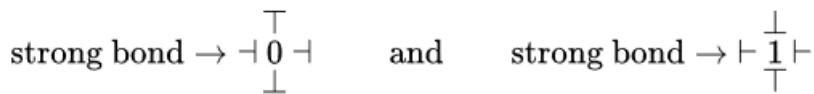


**Fig.1.16:** Concept of causality with Gyrator element

**Junctions:** All the efforts are equal in a 0-junction; all the flows are equal in a 1-junction. Therefore, the effort in a 0-junction can be caused due to only one bond, and similarly, the flow in a 1-junction can be caused due to only one bond. So, the causality of every other bond is determined if the causality of one bond is known. That one bond is called the 'strong bond'



## 1.4 RESEARCH OBJECTIVE

The present dissertation work explores the ability of bondgraph to model a three-dimensional, high speed track, subjected to varying speeds, and simulation of the same. As Bondgraph offers flexibility in modelling and generation of system equations, a modal model of the concrete slabs under the track is created in 3-D. The bondgraph model is easily modifiable which makes it an ideal tool for system modelling and generation of equations. The equations generated are generally used for generalised displacement as state variable. SYMBOLS Shakti is used for the bondgraph modelling and simulation.

The research's objective is:

1. To create a three-dimensional bond graph model of the concrete slab and sub grade system.
2. Simulation of vertical dynamics of high-speed railway track system.
3. Study the effect of vertical dynamics by varying the operational speed of the high-speed train.

## **1.5 ORGANIZATION OF THESIS**

The chapters of the thesis are arranged in the following manner.

Chapter 1 discusses about the basics of high-speed rail and track, and bondgraph modelling. Chapter 2 discussion of literature review. Chapter 3 presents the generation of bondgraph models of concrete slab - subgrade system. Chapter 4 presents simulation study. Chapter 5 deals with results and discussion and concludes along with some scope for future work.

## CHAPTER 2

### LITERATURE REVIEW

Various researchers have studied and computationally interpreted physically working models using the bond graph software. In the last few decades, extensive research has been carried out on various aspects of railway vehicle dynamics. Keeping in view the scope and objective of the present research, the literature study has been broadly focused on Track system interaction modelling, beams subjected to moving loads models, and bond graph models of Rail vehicle system.

**(Karmakar et al, 1990) [1]** have modelled Electric Overhead Travelling (EOT) cranes subjected to severe dynamic loading, using bond graph technique. A structural bond graph model of the EOT crane, subjected to a moving load, in terms of the hoisting trolley, was developed and simulated for three critical crane operations, namely, load hoisting, braking during load lowering and carriage motion over three types of rail joints. Subsequently, the bending stresses in the girder and tension in the ropes of the hoisting trolley were found out.

**(Zeng et. al, 1994) [3]** have described the bond graph modelling technique for vehicle-bridge coupling system. The vehicle system has been considered as a multiple rigid-body model and the bridge with single-span has been considered as a simply supported Bernoulli-Euler beam. The track has been simplified as a lumped parameter system and the effective rail and sleeper masses have been included in the vehicle-bridge coupling model. Finally, the 'dynamic responses of a freight vehicle-bridge system and wheel / rail impact forces have been investigated. In the findings of this paper, impact forces between wheel and rail have been strongly affected by the changes of vehicle speed and static wheel load, but have been slightly affected by the changes of primary suspension stiffness. The acceleration of bridge increases as vehicle speed increases and it has been unaffected by changes in primary suspension stiffness

(Nielsen et. al, 1995) [4] have investigated the vertical dynamic behaviour for a railway bogie moving on a rail which has been discretely supported via rail pads by sleepers resting on an elastic foundation. The transient interaction problem has been numerically solved by use of an extended state-space vector approach in conjunction with a complex modal superposition for the track. Application examples have been given in which the influences of three types of practically important imperfections in the compound vehicle/track system have been investigated. The first is a sinusoidal corrugation of the railhead and the second a skid ~at on the wheel tread (a wheel flat). The third imperfection is a case where a single sleeper has lost its support due to erosion of the ballast. Physical explanations of the calculated interaction behaviour have been given.

(Chan et. al, 2002) [6] have presented an overview of the present status of electric and hybrid vehicles worldwide and their state of the art, with emphasis on the engineering philosophy and key technologies. The importance of the integration of technologies electronics, automobile, electric motor drive, controls and energy storage and also the importance of the integration of society strength from government, research institutions, industry, electric power utilities, and transportation authorities were addressed. The key issue of HEV is how to optimize the multiple energy sources to obtain best performance at lower cost. FCEV would have a long-term potential to be the conventional vehicle in the future because it has been almost zero emission and comparable driving range to ICEV. However, as it has been still in the early development stage today, the major setback of FCEV has been how to develop low-cost FC, efficient fuel processor, and refuelling system. A proper engineering philosophy has been essential for the guidance of strategic development of EVs.

(Kumaran et. al, 2002) [7] have discussed the dynamic response of a typical prestressed concrete rail track sleeper due to wheel-track interaction dynamics, involving wheel and rail imperfections, under various parametric conditions. The interaction dynamics of the vehicle and track has been first carried out in the time domain using MSC/NASTRAN. Using the resulting load time histories on an isolated sleeper, a detailed finite element model of the sleeper has been used to analyse its dynamic behaviour. The dynamic amplification factors for deflection, ballast pressure and bending moments have been evaluated at the critical section

(rail-seat and centre) for various exciting frequencies under different vehicle–track parametric conditions. The results provide a basis for improved and rational design of the sleeper.

**(Bureika et. al, 2002) [8]** have presented how the effects on maximum bending tensions at different locations in the track caused by simultaneous changes of the various parameters can be estimated in a rational manner. The dynamic of vertical interaction between a moving rigid wheel and a flexible railway track has been investigated. A round and smooth wheel tread and an initially straight and non-corrugated rail surface have been assumed in the present optimisation study. Asymmetric linear three-dimensional beam structure model of a finite length of the track has been suggested including rail, pads, sleepers and ballast with spatially non-proportional damping. Transient bending tensions in sleepers and rail have been calculated. The influence of eight selected track parameters on the dynamic behaviour of the track has been investigated. A two-level fractional factorial design method has been used in the search for a combination of numerical levels of these parameters making the maximum bending tensions the minimum. Finally, the main conclusions have been given.

**(Kumaxl et. al, 2005) [10]** have presented, a numerical simulation of the lateral dynamic behaviour of a railway vehicle. A typical Indian railway vehicle of the AC/EMU/T (Alternating Current/Electrical Multiple Unit/Trailer) type running on broad gauge track has been chosen for the analysis. A 17 degree of freedom (dof) linear mathematical model of the vehicle has been used for the analysis, Kalker's creep theory has been applied to evaluate the tangential contact forces acting between wheel and rail. Linear governing equations of motion of the vehicle on a straight track have been solved. Natural frequencies have been determined from the above mathematical model. Dynamic response studies were carried out in the frequency domain with power spectral densities of track gauge and alignment irregularities as input.

**(Rastogi et. al, 2009) [12]** have presented a study that deals with the effects of railway track imperfections on dynamic behaviour, and investigated the effect of vehicle speed and the rail irregularity on ride comfort through numerical simulation. The numerical simulation of the vertical dynamic behaviour of a typical railroad vehicle was done by modelling through bond graph technique. The model consisted of 17 degree of freedom with wheel set, bogie and car.

For assessment of ride comfort Sperling ride index used by Indian Railway was calculated using filtered RMS accelerations. The ride characteristics of the vehicle provided assessment of the dynamic behaviour of the vehicle through analysis of accelerations at the vehicle body, whereas ride comfort assessed the influence of vehicle dynamic behaviour on the human body.

**(Gustafsson et. al, 2009) [13]** have investigated the dynamic response of railway bridges for high-speed trains and developed a reduced model that can be used early in a project, to provide a quick dynamic analysis of bridges with several spans. The reduced model was based on the fact that the fundamental dynamic behaviour of certain type of bridges may be described by the dynamic behaviour of 2-dimensional Bernoulli beam elements. The bridge model was developed as a MATLAB function and consists of a selectable number of Bernoulli beam elements. Three different approaches of modelling the train load were compared. The first method of modelling the train was made as moving point-loads, the second as a distributed load and the third as a separate mass and spring model.

**(Rastogi et. al, 2009) [14]** have considered a complete model of a railway vehicle, which has been assembled from wheel sets, car body and intermediate structure which have been flexible, and which have been connected by components such as springs and dampers. Similarly, the vehicle has been considered to run on a track, which has a complex structure with elastic and dissipative properties. The track can be modelled as a continuous structure with moving interface at the point of contact, whereas the interaction between the wheel and the rail has been dependent on the relative motion. In calculating the coupled vehicle and track dynamics, Hertzian contact theory has been applied to calculate the normal force between the wheel and the rails.

**(Goicolea et. al, 2010) [15]** have developed models for calculation of vertical dynamic traffic load effects on railway track infrastructures, and applications for evaluating the comparative performance of ballast and slab track designs. The calculations have been based on dynamic finite element models with direct time integration and contact algorithms between wheel and rail in order to consider the rail-car interaction. For capturing the dynamic effects has been an adequate representation of irregularities of the track. The 2D spatial discretization were selected



as the optimal decisions. The results obtained include wheel-rail contact forces, forces transmitted to the bogie by primary suspension and forces transmitted to the infrastructure (sleeper or slab) by the rail pads.

(**Nguyen et. al, 2011**) [16] have carried out the study to develop and calibrate the optimal models for the objectives of this work. In particular, quarter bogie model for vehicle, rail-wheel contact with Lagrangian multiplier method, 2D spatial discretization were selected as the optimal decisions. Furthermore, the 3D model of coupled vehicle-track also has been developed to contrast the results obtained in the 2D model. The calculations were carried out in the time domain and envelopes of relevant results were obtained for several track profiles and speed ranges. Distributed elevation irregularities were generated based on power spectral density (PSD) distributions. The results obtained include the wheel-rail contact forces, forces transmitted to the bogie by primary suspension. The latter loads have been relevant for the purpose of evaluating the performance of the infrastructure.

(**Lei et. al, 2016**) [17] have established a model for dynamic analysis of the vehicle-track nonlinear coupling system by the finite element method. The whole system has been divided into two subsystems: the vehicle subsystem and the track subsystem. Coupling of the two subsystems has been achieved by equilibrium conditions for wheel-to-rail nonlinear contact forces and geometrical compatibility conditions. To solve the nonlinear dynamics equations for the vehicle-track coupling system, a cross iteration algorithm and a relaxation technique have been presented. Examples of vibration analysis of the vehicle and slab track coupling system induced by China's high-speed train CRH3 have been given. In the computation, the influences of linear and nonlinear wheel-to-rail contact models and different train speeds have been considered. It has been found that the cross-iteration algorithm and the relaxation technique have the following advantages: simple programming; fast convergence; shorter computation time; and greater accuracy. The analysed dynamic responses for the vehicle and the track with the wheel-to-rail linear contact model have been greater than those with the wheel-to-rail nonlinear contact model, where the increasing range of the displacement and the acceleration has been about 10%, and the increasing range of the wheel to-rail contact force has been less than 5%.

(Cao et. al, 2017) [18] have carried out the dynamic analysis of three-dimensional high-speed train-track model using moving element method. The train comprised of a car-body supported by a secondary suspension system to a bogie. The bogie, has been, in turn, connected to wheel-sets through a primary suspension system. A total of 16 degrees of freedom have been employed to describe the vertical, lateral, rolling, pitching, and yawing displacements of the car-body, the bogie, and the wheel-sets. The Hertzian contact and Kalker's linear theory have been used to account for the vertical and lateral contact forces between the wheels and rails. Two rails have been modelled as two Euler–Bernoulli beams resting on a viscoelastic foundation. The moving element method has been extended to establish the coupling formulations of the mass, damping, and stiffness matrices in vertical and lateral directions, where the element matrices have been formulated based on a convected coordinate system attached to the moving vehicle. The dynamic amplification factor has been defined as the ratio of the maximum dynamic contact force to the static load at the contact point between the wheel and the rail. To illustrate the benefits of the proposed three-dimensional train-track model, several numerical examples have been performed in this study to present the effects of the train speed, the resonance phenomenon, the track irregularity, and track stiffness variations along the track and across the track width on the dynamic amplification factor of the high-speed train.

(Kumar et. al, 2018) [20] have proposed a large variety of models and have been used for many different circumstances. A combined vehicle-track bond graph model has been developed to study the wheel/ track impact. The rail flexibility has been considered, modelling rail as a flexible Euler Bernoulli beam with discrete support. Non-linearity in pad and ballast behaviour and wheel-rail contact has also been taken into considerations while developing the combined model. It has been noticed from simulation results that; a linear track model has been found to be inappropriate for wheel/track interaction problems due to the extremely large value of impact load. The obtained results further lead to provide a good all-inclusive view of the contact dynamics of the wheel/track interface.

## CHAPTER 3

# COMPUTATIONAL MODELS OF HIGH-SPEED TRACK AND METHODOLOGY

The components of high-speed track were modelled using SYMBOLS Shakti software. The track consists of concrete slab, cement-asphalt mortar, and sub grade. The physical model of the system is as shown below.

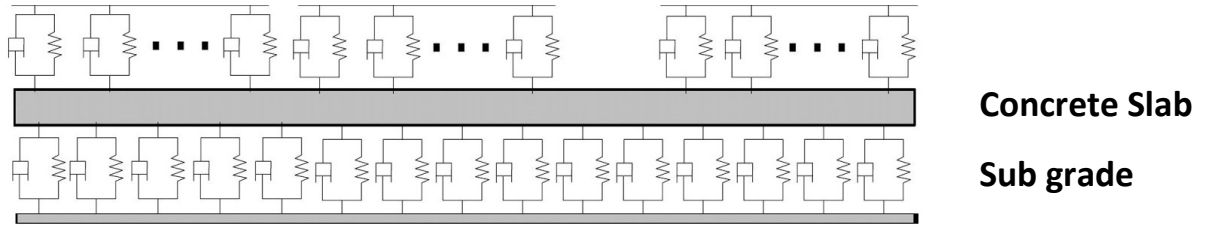


**Fig.3.1:** Concrete Slab - Sub grade model, connected with spring damper system.

Concrete slab is connected to the subgrade, and two parallel concrete slabs are inter connected using cement-asphalt mortar. All the connections are in the form of spring-damper systems. In the spring-damper system, the spring (C), denotes the stiffness properties, and the damper (R), denotes structural damping.

### 3.1 Numerical Modelling

In this paper the track, i.e., the concrete slab is modelled as Euler-Bernoulli beam. If the transverse deflection of the beam is taken as  $z_s(x,t)$ , where  $x$  denotes the longitudinal position of the beam. Then, the partial differential equation of the beam can be derived and given as –

$$EI_s \frac{\partial^4 z_s(x,t)}{\partial x^4} + \rho_r A_r \frac{\partial^2 z_s(x,t)}{\partial x^2} = P_c(t) \delta(x - x_w)$$

(3.1)

Here,

$EI_s$  - Vertical bending stiffness of concrete slab

$\rho_s$  - Density of concrete slab

$A_s$  - Area of cross section of the concrete slab

$P_c(t)$  - Contact force at the wheel/rail/slab interface.

$x$  - The longitudinal position of the concrete slab with respect to the left end support of the beam.

$x_w$  - The position of the wheel

$\delta(\cdot)$  - Dirac's delta function.

The partial differential equation is converted into normal derivatives by variable-separation method. Solution by this method comes out to be an infinite sum of product of shape function  $Y_i(x)$  and modal amplitude  $q_i(t)$ , which represents the vertical motion of the slab. In the present analysis total 5 modes are considered. The displacement of the rail beam at  $x$  from the beam end at time  $t$  is given by

$$z_r(x, t) = \sum_{i=1}^{NM} Y_i(x) q_i(t)$$

(3.2)

where NM is the number of modes

Both the ends of the concrete slab beam are pivoted, therefore, at both the ends, the deflections and the bending moments are equal to zero. Applying these boundary conditions, shape function and natural frequencies for  $i^{th}$  mode, are obtained, as given by Eq (3.3) and Eq. (3.4) respectively. [19]

$$Y_i(x) = \sin\left(\frac{i\pi x}{L_s}\right)$$

(3.4)

$$\omega_i = \left(\frac{i\pi x}{L_s}\right)^2 \sqrt{\frac{EI_s}{\rho_s A_s}} \quad (3.5)$$

where,

$L_s$  is the length of the concrete slab

Substituting Eq. (3.4) to Eq. (3.5) and integrating with respect to  $x$  along the length of beam, considering the orthogonality property of shape functions, one obtains Eq. (3.6).

$$m_i \ddot{q}_i + k_i q_i = P_c(t) Y_i(x_w) \quad (3.6)$$

where,  $m_i$  is the modal mass and  $k_i$  is the  $i^{\text{th}}$  modal stiffness

$$m_i = \frac{\rho_s A_s L_s}{2} \quad i = 1, 2 \dots NM \quad (3.7)$$

$$k_i = m_i \omega_i^2 \quad i = 1, 2 \dots NM \quad (3.8)$$

The modal momentum is given by the expression –

$$p_i = m_i \dot{q}_i \quad (3.9)$$

Therefore the equation (3.6) can be written as –

$$\frac{dp_i}{dt} = -k_i q_i + P_c(t) Y_i(x_w) \quad (3.10)$$

and

$$\frac{dq_i}{dt} = \frac{p_i}{m_i} \quad (3.11)$$

This reduces the equation, which is an  $i^{th}$  modal equation, in the form of  $q_i$  and  $p_i$ , into 2, first order state equations.

The equation 3.4 is used in the expression of transformer element in the bond graph. Similarly, equations (3.7) and (3.8) are used in the expression of stiffness properties of the concrete slab

### 3.2 Bond Graph Modelling

The resulting modal bond graph model for the concrete slab/sub grade system is as shown below

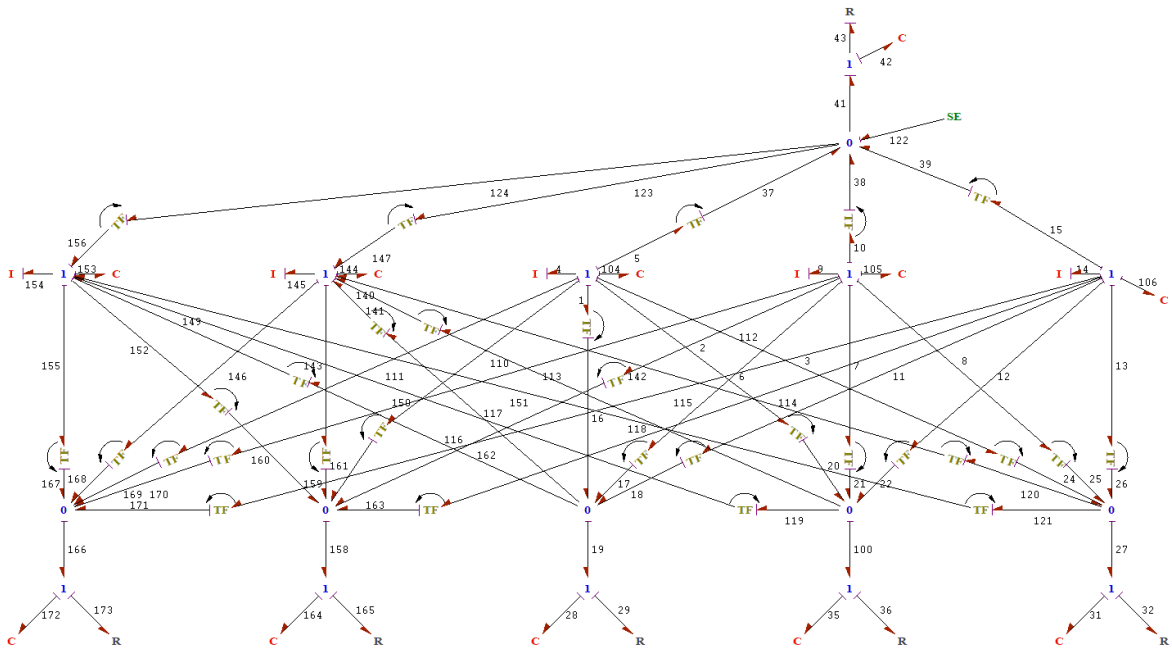


**Fig.3.2:** Bond graph model of the concrete slab and sub grade system

Here, C172, C164, C28, C35, and C31, represent the stiffness properties of the sub grade. R173, R1655, R29, R36, and R32, represent the damping properties of the sub grade. The 1-elements, joined to the 0-elements, by transfer functions represent the nodes of the beam (concrete slab).

When the bond graph shown above, for a single rail, is to be converted in 3-D, a system of springs and dampers denoting the Cement-asphalt mortar is used to join the two rails to model the whole track. The bond graph model for the same is shown below –

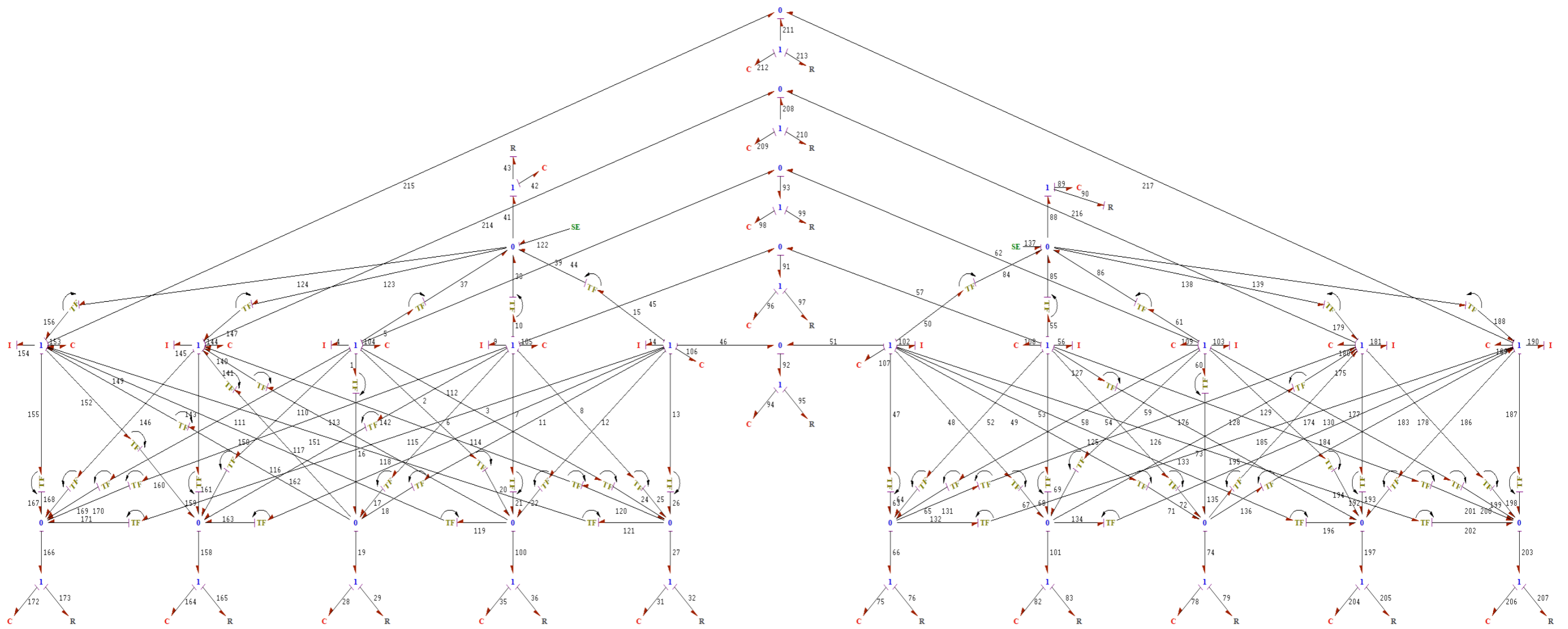


**Fig.3.3:** Three-dimensional Bond graph modal model of the concrete slab and sub-grade system, subjected to a constant moving load



It is a three-dimensional modal model of the concrete slab – sub grade system, subjected to moving load of the train. The concrete slab is divided into five modes.

### **3.3 Methodology**

To construct a modal model for the concrete slab – sub grade system, for high speed tracks, the beam (concrete slab) was divided into five modes. The contact between concrete slab and sub grade was considered as a spring-damper system, where the spring and damper, represented stiffness and damping properties, respectively. The contact between the moving load and the concrete slab is modelled in a similar fashion. The two concrete slabs under the two parallel rails, connected with cement-asphalt mortar, are modelled in a way that, the same modes of both slabs are connected with the help of a spring damper system, representing the properties of cement-asphalt mortar.

Equation 3.4, 3.5, 3.7, and 3.8, are used to write expressions for the bond graph elements. After that, the bond graph was checked for errors and warning, and then the equations were generated successfully. The bond graph system was then compiled and simulated.

## **CHAPTER 4**

### **SIMULATION STUDY**

The results obtained, in the form of graphs are shown in this section, for the simulation of the bond graph shown in figure 3.3. The interpretation of the results is discussed in the next chapter.

After defining all the expressions in the bond graph model and after the generation of all the equations successfully, the bond graph is then simulated. All the values of parameters are to be entered for the generation of graphs in the simulation window, and an appropriate time duration is chosen for the same.

The values of all the properties of the elements, used in the expressions and in the final calculations of the model, during the simulation are shown in the table below –

<b>Properties</b>	<b>Values</b>
Stiffness properties of Sub grade (C <sub>sub</sub> )	$60 \times 10^6$ N/m
Damping properties of Sub grade (R <sub>sub</sub> )	$90 \times 10^3$ Ns/m
Density of Concrete Slab ( $\rho$ )	$2500 \text{ kg/m}^3$
Length of Concrete Slab (L)	15 m
Area of cross section of a single Concrete Slab (A)	$0.435 \text{ m}^2$
Stiffness properties of Concrete slab (C <sub>contact</sub> )	$87 \times 10^9$ N/m
Stiffness properties of Cement-Asphalt Mortar (C <sub>lat</sub> )	$90 \times 10^7$ N/m
Damping properties of Cement-Asphalt Mortar (R <sub>lat</sub> )	$83 \times 10^3$ Ns/m
Flexural Rigidity of Concrete Slab (EI)	$13.25 \times 10^6 \text{ Nm}^2$
Static load acting on the beam (Concrete slab)	$80 \times 10^3$ N

**Table 4.1:** Material properties of the components of high-speed track

The parameters mentioned above are used during the simulation of the final bond graph. The graphs generated henceforth can be altered by varying the values of parameters in the “parameters” section in the simulation window. The trend and the time of operation for the system to become stable, or tend towards becoming stable, is primary concern.

At various operational speeds, ranging from 200 kmph to 500kmph, the simulation is run, for 10 seconds, to obtain the deflection curves at different modes of the beam (concrete slab), the sub grade, and also at the Cement-asphalt mortar joint, for lateral deflection. The Fast Fourier Transform (FFT) is generated for the same, at different modes

and at different speeds, for a time duration of 40 seconds, which in turn gives the magnitude versus frequency graphs.

#### 4.1 Case I - Deflection in Concrete Slab – 4.1.1 Mode – 1

Velocity 200 kmph

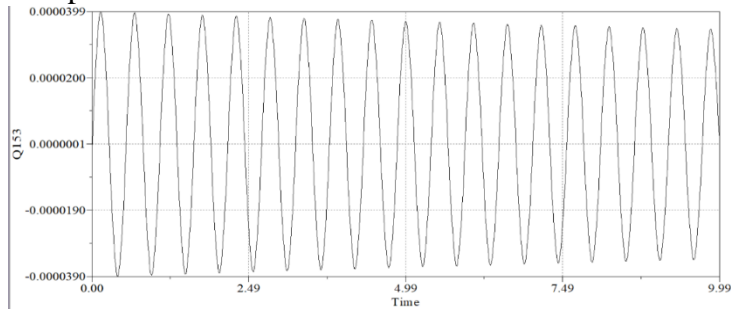


**Fig.4.1:** Deflection (m) vs Time (s) graph for Mode 1 of Concrete Slab at 200 kmph

Velocity 400 kmph

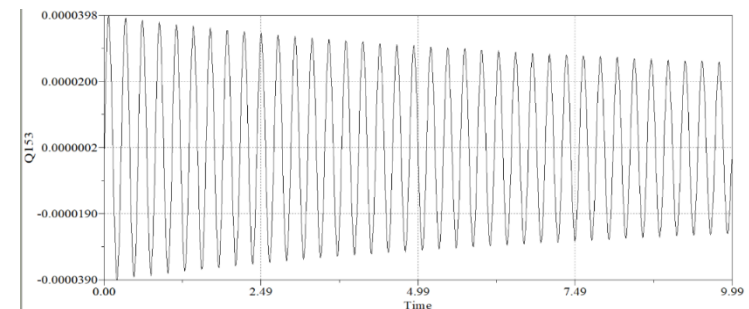


**Fig.4.3:** Deflection (m) vs Time (s) graph for Mode 1 of Concrete Slab at 400 kmph

Velocity 300 kmph

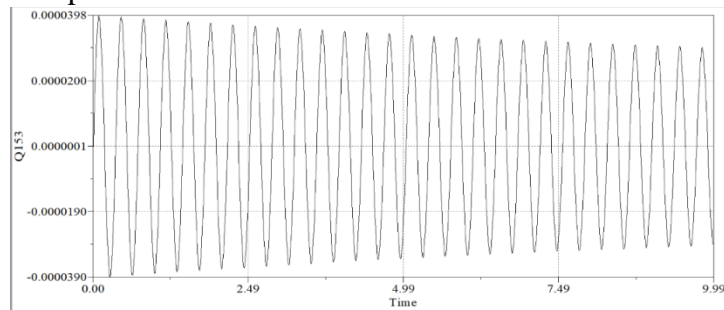


**Fig.4.2:** Deflection (m) vs Time (s) graph for Mode 1 of Concrete Slab at 300 kmph

Velocity 500 kmph

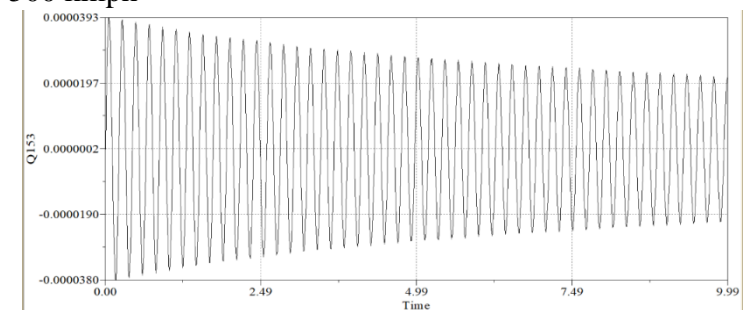


**Fig.4.4:** Deflection (m) vs Time (s) graph for Mode 1 of Concrete Slab at 500 kmph

In the above graphs it can be observed that the maximum average deflection at mode 1, for all four velocities, is 0.0392 mm, which dies out eventually, more rapidly at the velocity 500 kmph.

### 4.1.2 Mode – 2

Velocity 200 kmph

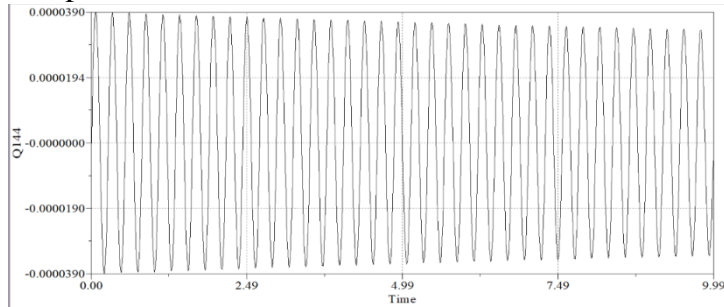


**Fig.4.5:** Deflection (m) vs Time (s) graph for Mode 2 of Concrete Slab at 200 kmph

Velocity 400 kmph

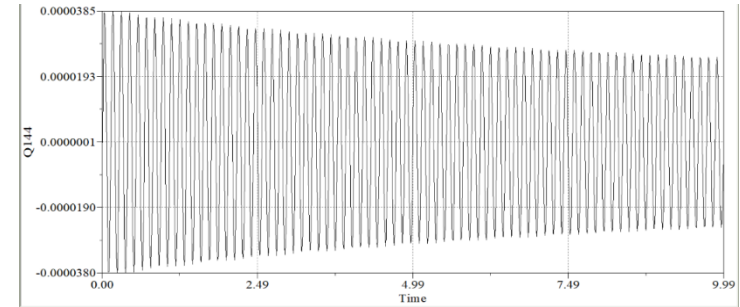


**Fig.4.7:** Deflection (m) vs Time (s) graph for Mode 2 of Concrete Slab at 400 kmph

Velocity 300 kmph

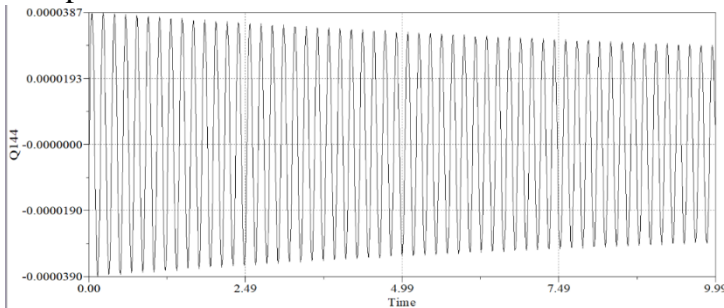


**Fig.4.6:** Deflection (m) vs Time (s) graph for Mode 2 of Concrete Slab at 300 kmph

Velocity 500 kmph

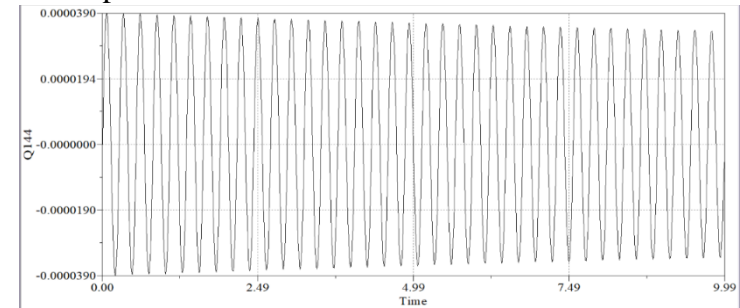


**Fig.4.8:** Deflection (m) vs Time (s) graph for Mode 2 of Concrete Slab at 500 kmph

In the above graphs it can be observed that the maximum average deflection at mode 1, for all four velocities, is 0.0387 mm, which dies out eventually, more rapidly at the velocity 500 kmph.

### 4.1.3 Mode – 3

Velocity 200 kmph

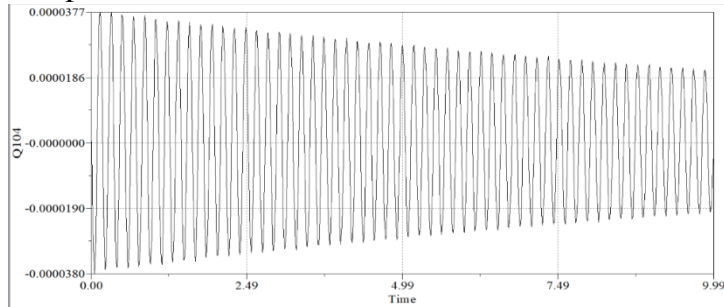


**Fig.4.9:** Deflection (m) vs Time (s) graph for Mode 3 of Concrete Slab at 200 kmph

Velocity 400 kmph

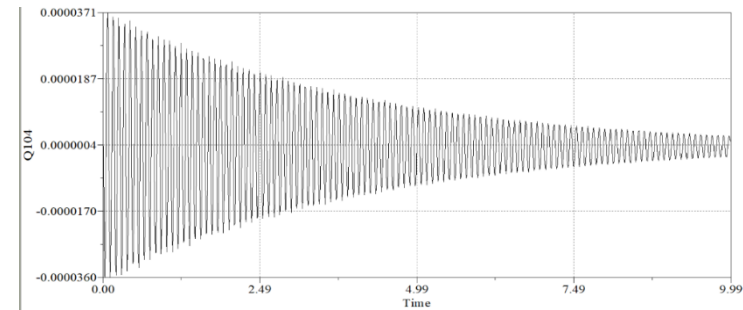


**Fig.4.11:** Deflection (m) vs Time (s) graph for Mode 3 of Concrete Slab at 400 kmph

Velocity 300 kmph

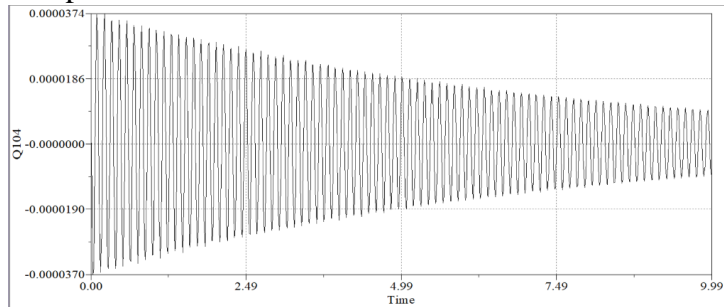


**Fig.4.10:** Deflection (m) vs Time (s) graph for Mode 3 of Concrete Slab at 300 kmph

Velocity 500 kmph

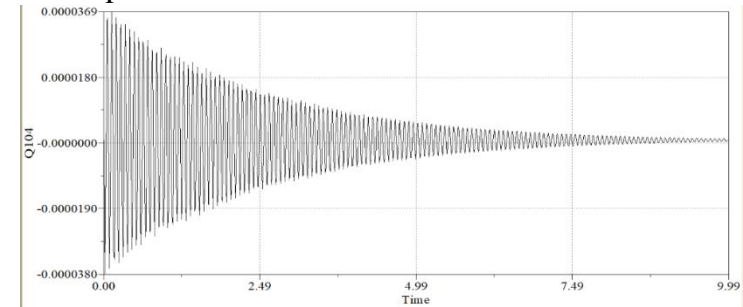


**Fig.4.12:** Deflection (m) vs Time (s) graph for Mode 3 of Concrete Slab at 500 kmph

In the above graphs it can be observed that the maximum average deflection at mode 1, for all four velocities, is 0.0372 mm, which dies out eventually, more rapidly at the velocity 500 kmph.

#### 4.1.4 Mode – 4

Velocity 200 kmph

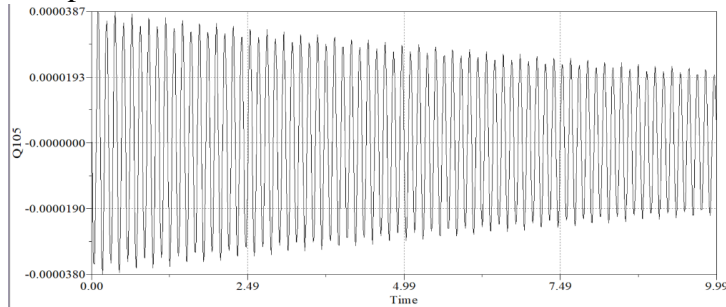


**Fig.4.13:** Deflection (m) vs Time (s) graph for Mode 4 of Concrete Slab at 200 kmph

Velocity 400 kmph

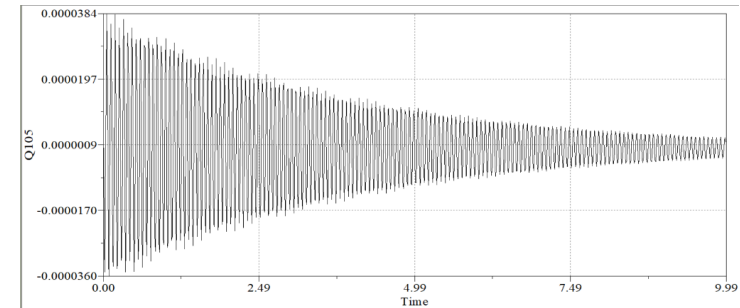


**Fig.4.15:** Deflection (m) vs Time (s) graph for Mode 4 of Concrete Slab at 400 kmph

Velocity 300 kmph

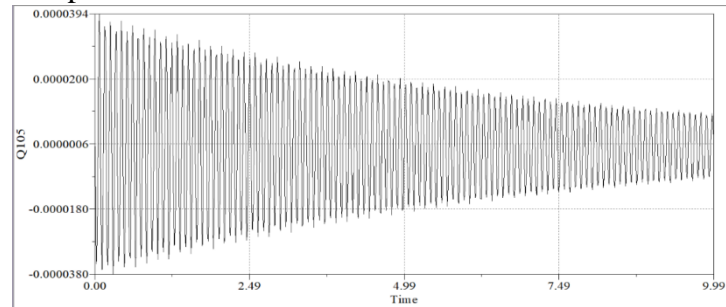


**Fig.4.14:** Deflection (m) vs Time (s) graph for Mode 4 of Concrete Slab at 300 kmph

Velocity 500 kmph

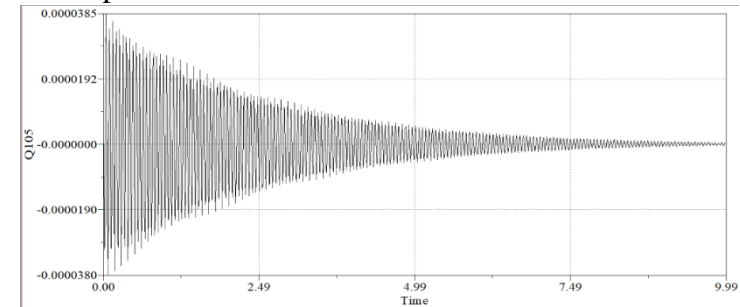


**Fig.4.16:** Deflection (m) vs Time (s) graph for Mode 4 of Concrete Slab at 500 kmph

In the above graphs it can be observed that the maximum average deflection at mode 1, for all four velocities, is 0.0381 mm, which dies out eventually, more rapidly at the velocity 500 kmph



### 4.1.5 Mode – 5

Velocity 200 kmph

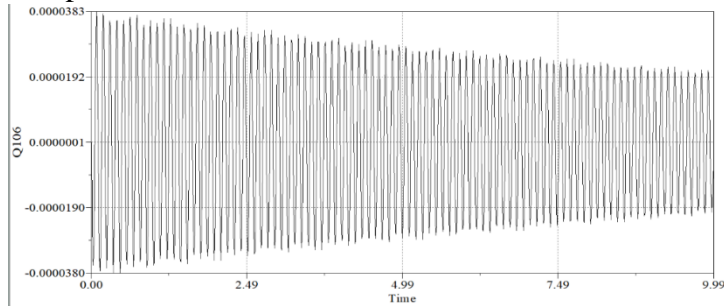


**Fig.4.17:** Deflection (m) vs Time (s) graph for Mode 5 of Concrete Slab at 200 kmph

Velocity 400 kmph

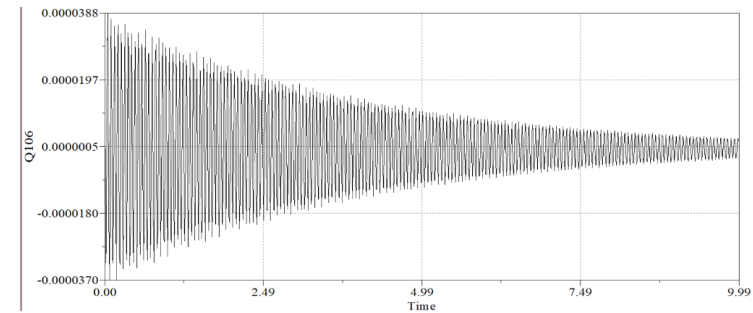


**Fig.4.19:** Deflection (m) vs Time (s) graph for Mode 5 of Concrete Slab at 400 kmph

Velocity 300 kmph

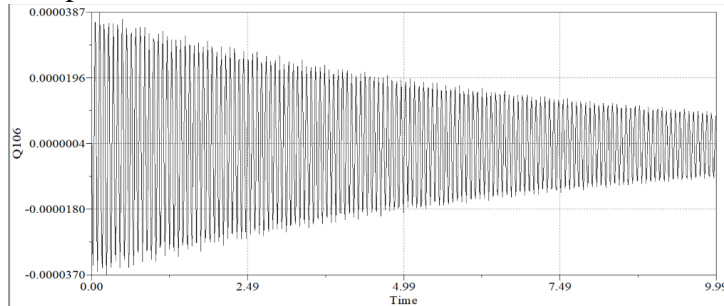


**Fig.4.18:** Deflection (m) vs Time (s) graph for Mode 5 of Concrete Slab at 300 kmph

Velocity 500 kmph

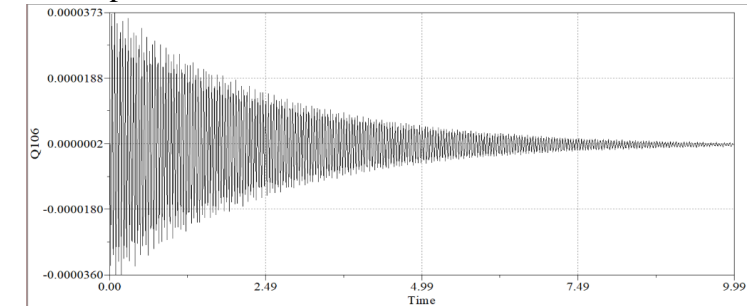


**Fig.4.20:** Deflection (m) vs Time (s) graph for Mode 5 of Concrete Slab at 500 kmph

In the above graphs it can be observed that the maximum average deflection at mode 1, for all four velocities, is 0.0376 mm, which dies out eventually, more rapidly at the velocity 500 kmph.

## 4.2 Case II - Deflection in Sub grade–

### 4.2.1 Mode – 1

Velocity 200 kmph

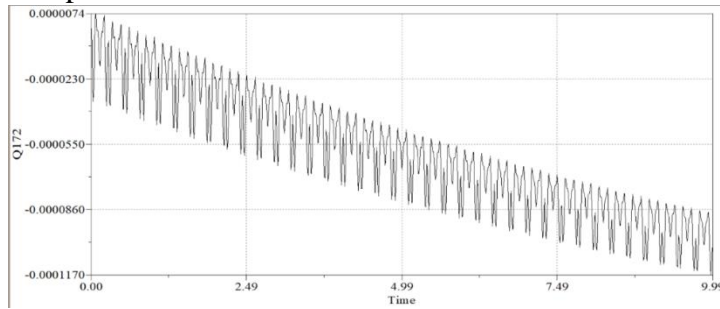


**Fig.4.21:** Deflection (m) vs Time (s) graph for Mode 1 of Sub grade at 200 kmph

Velocity 400 kmph

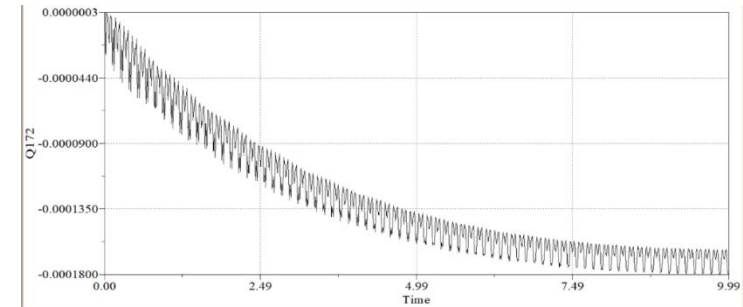


**Fig.4.23:** Deflection (m) vs Time (s) graph for Mode 1 of Sub grade at 400 kmph

Velocity 300 kmph

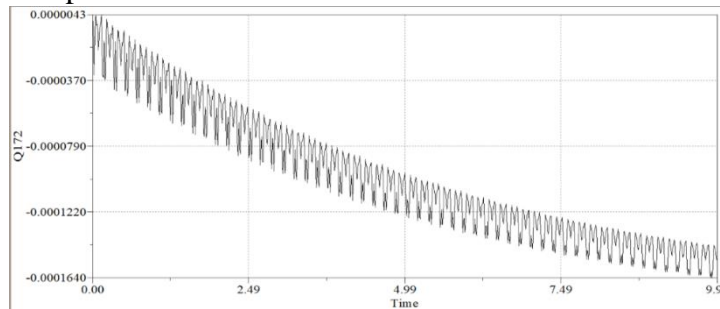


**Fig.4.22:** Deflection (m) vs Time (s) graph for Mode 1 of Sub grade at 300 kmph

Velocity 500 kmph

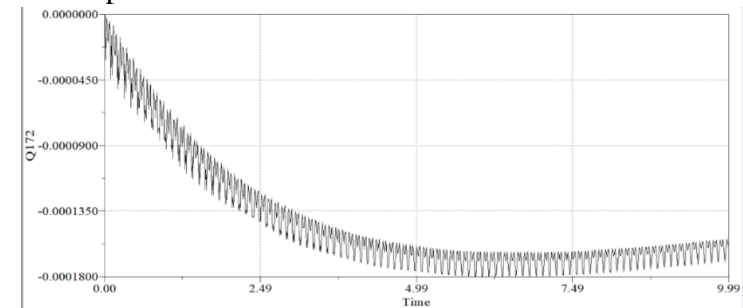


**Fig.4.24:** Deflection (m) vs Time (s) graph for Mode 1 of Sub grade at 500 kmph

In the above graphs it can be observed that the maximum average deflection at mode 1, for all four velocities, is 0.1632 mm, which dies out eventually, more rapidly at the velocity 500 kmph.

#### 4.2.2 Mode – 2

Velocity 200 kmph

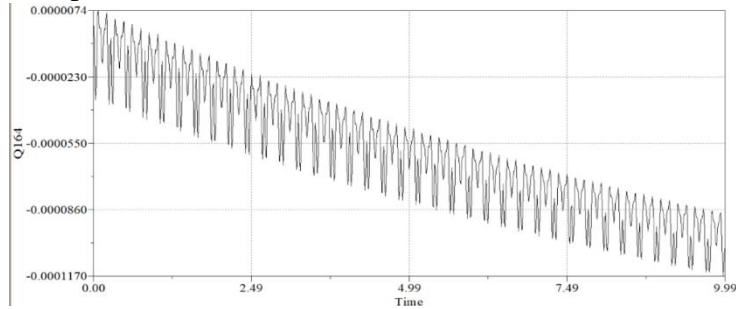


**Fig.4.25:** Deflection (m) vs Time (s) graph for Mode 2 of Sub grade at 200 kmph

Velocity 400 kmph

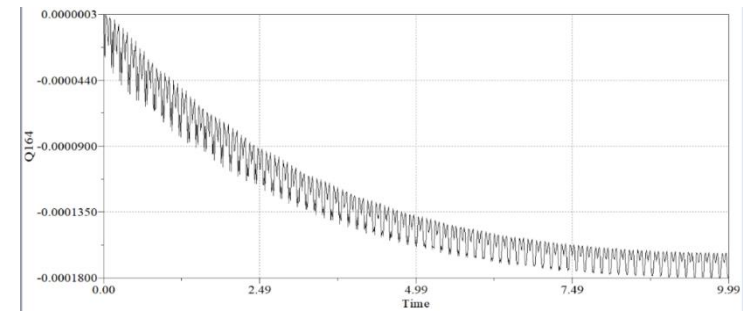


**Fig.4.27:** Deflection (m) vs Time (s) graph for Mode 2 of Sub grade at 400 kmph

Velocity 300 kmph

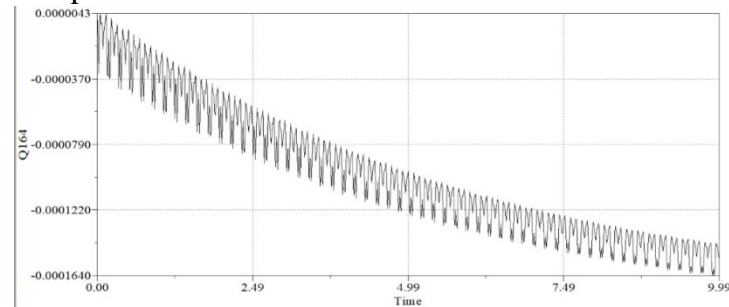


**Fig.4.26:** Deflection (m) vs Time (s) graph for Mode 2 of Sub grade at 300 kmph

Velocity 500 kmph

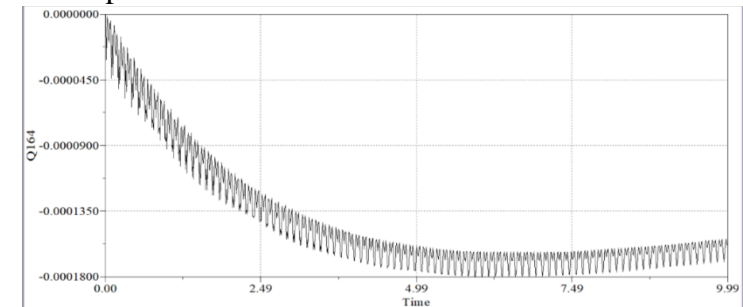


**Fig.4.28:** Deflection (m) vs Time (s) graph for Mode 2 of Sub grade at 500 kmph

In the above graphs it can be observed that the maximum average deflection at mode 1, for all four velocities, is 0.1632 mm, which dies out eventually, more rapidly at the velocity 500 kmph.

### 4.2.3 Mode – 3

Velocity 200 kmph

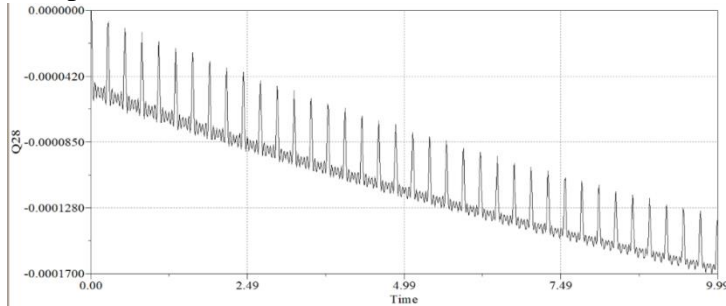


**Fig.4.29:** Deflection (m) vs Time (s) graph for Mode 3 of Sub grade at 200 kmph

Velocity 400 kmph

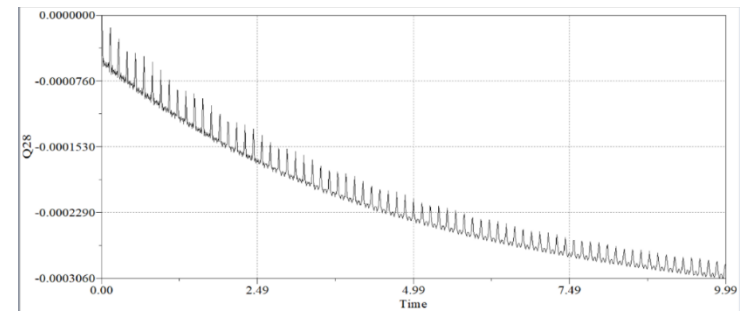


**Fig.4.31:** Deflection (m) vs Time (s) graph for Mode 3 of Sub grade at 400 kmph

Velocity 300 kmph

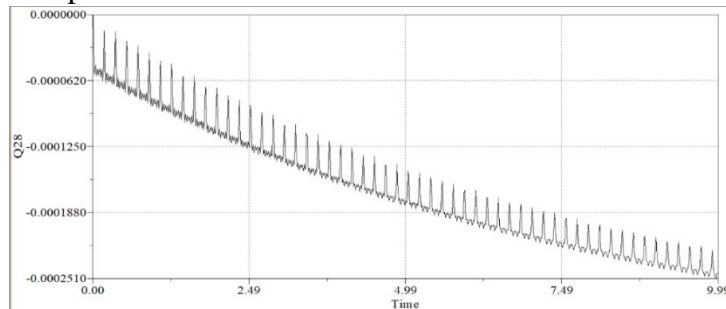


**Fig.4.30:** Deflection (m) vs Time (s) graph for Mode 3 of Sub grade at 300 kmph

Velocity 500 kmph

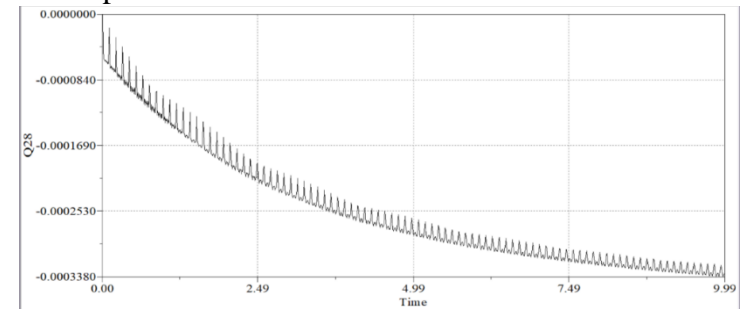


**Fig.4.32:** Deflection (m) vs Time (s) graph for Mode 3 of Sub grade at 500 kmph

In the above graphs it can be observed that the maximum average deflection at mode 1, for all four velocities, is 0.1632 mm , which dies out eventually, more rapidly at the velocity 500 kmph.

#### 4.2.4 Mode – 4

Velocity 200 kmph

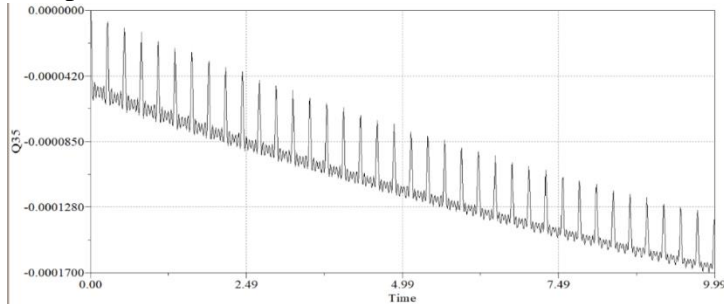


**Fig.4.33:** Deflection (m) vs Time (s) graph for Mode 4 of Sub grade at 200 kmph

Velocity 400 kmph

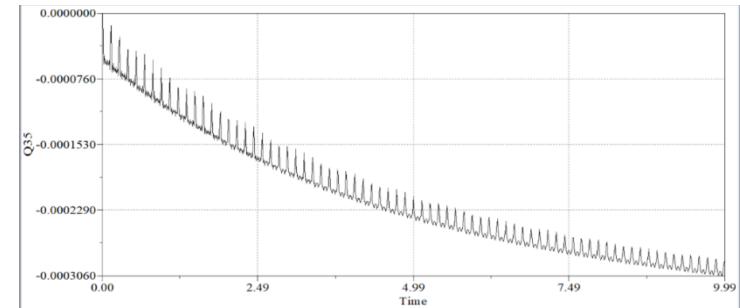


**Fig.4.35:** Deflection (m) vs Time (s) graph for Mode 4 of Sub grade at 400 kmph

Velocity 300 kmph

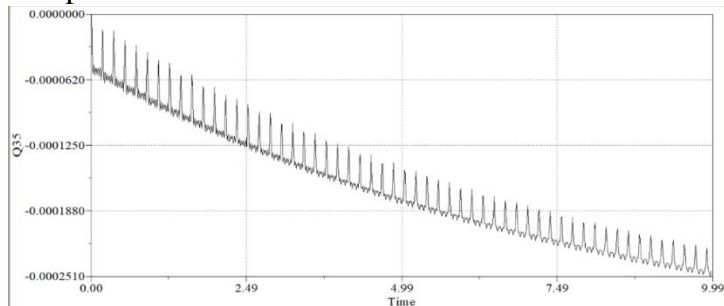


**Fig.4.34:** Deflection (m) vs Time (s) graph for Mode 4 of Sub grade at 300 kmph

Velocity 500 kmph

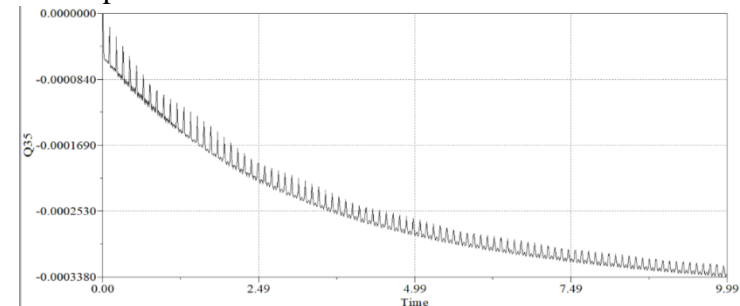


**Fig.4.36:** Deflection (m) vs Time (s) graph for Mode 4 of Sub grade at 500 kmph

In the above graphs it can be observed that the maximum average deflection at mode 1, for all four velocities, is 0.2662 mm, which dies out eventually, more rapidly at the velocity 500 kmph

#### 4.2.5 Mode – 5

Velocity 200 kmph

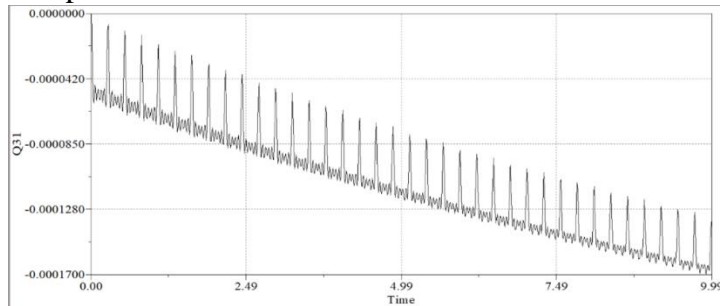


**Fig.4.37:** Deflection (m) vs Time (s) graph for Mode 5 of Sub grade at 200 kmph

Velocity 400 kmph

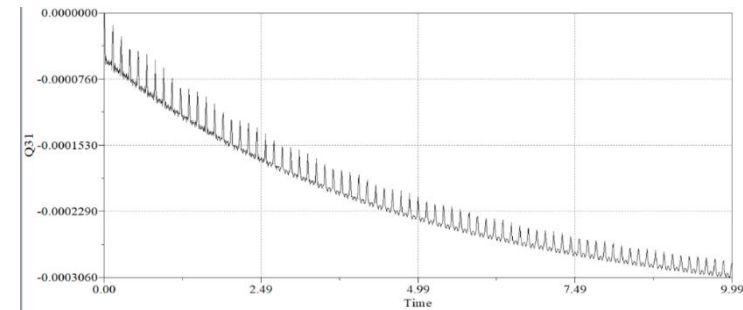


**Fig.4.39:** Deflection (m) vs Time (s) graph for Mode 5 of Sub grade at 400 kmph

Velocity 300 kmph

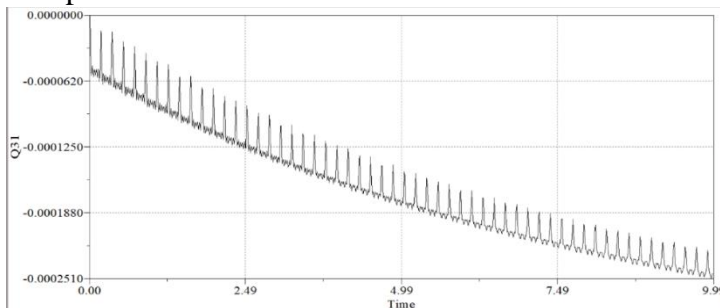


**Fig.4.38:** Deflection (m) vs Time (s) graph for Mode 5 of Sub grade at 300 kmph

Velocity 500 kmph

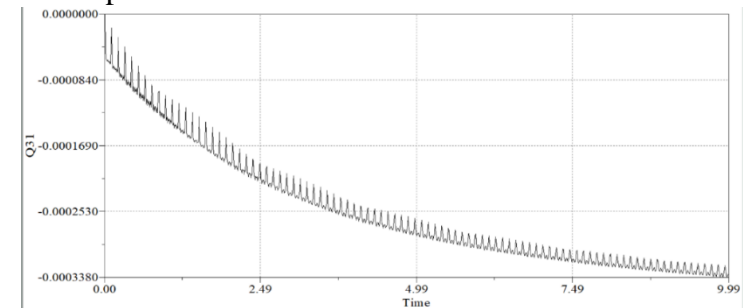


**Fig.4.40:** Deflection (m) vs Time (s) graph for Mode 5 of Sub grade at 500 kmph

In the above graphs it can be observed that the maximum average deflection at mode 1, for all four velocities, is 0.2662 mm, which dies out eventually, more rapidly at the velocity 500 kmph.

### 4.3 Case III -Lateral deflection between concrete slabs-

#### 4.3.1 Mode – 1

Velocity 200 kmph

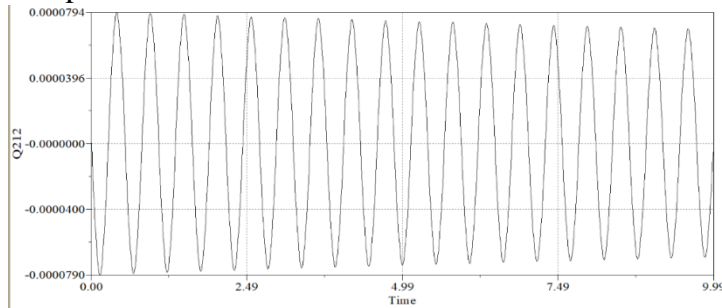


**Fig.4.41:** Deflection (m) vs Time (s) graph for Mode 1 of Concrete Slab at 200 kmph

Velocity 400 kmph

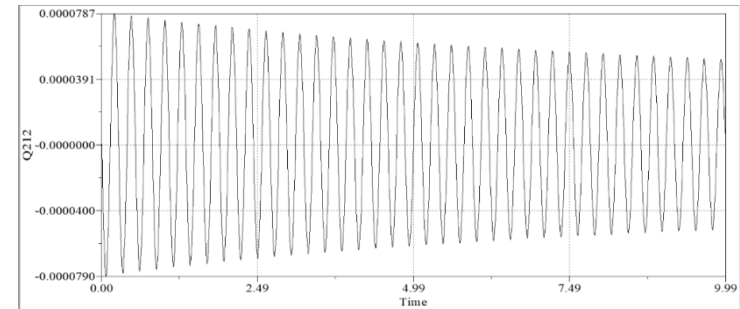


**Fig.4.43:** Deflection (m) vs Time (s) graph for Mode 1 of Concrete Slab at 400 kmph

Velocity 300 kmph

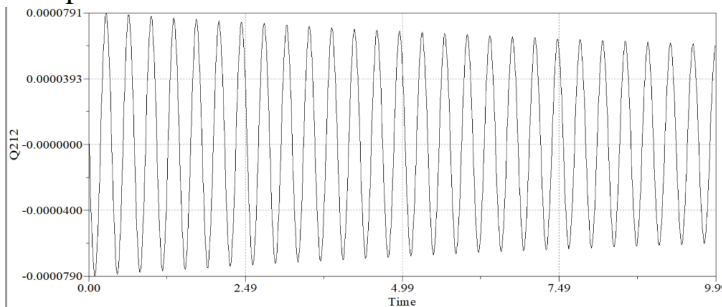


**Fig.4.42:** Deflection (m) vs Time (s) graph for Mode 1 of Concrete Slab at 300 kmph

Velocity 500 kmph

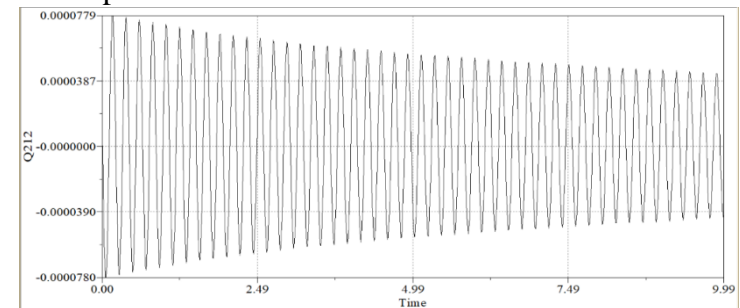


**Fig.4.44:** Deflection (m) vs Time (s) graph for Mode 1 of Concrete Slab at 500 kmph

In the above graphs it can be observed that the maximum average deflection at mode 1, for all four velocities, is 0.0392 mm , which dies out eventually, more rapidly at the velocity 500 kmph.

### 4.3.2 Mode – 2

Velocity 200 kmph

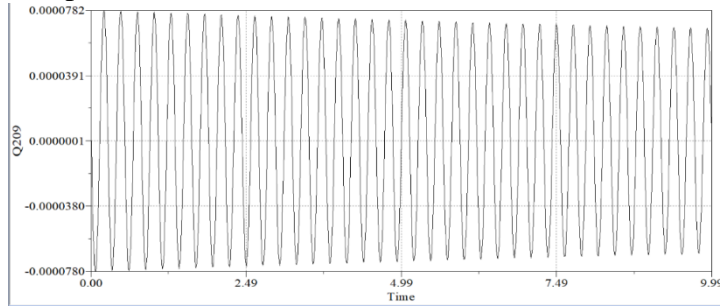


**Fig.4.45:** Deflection (m) vs Time (s) graph for Mode 2 of Concrete Slab at 200 kmph

Velocity 400 kmph

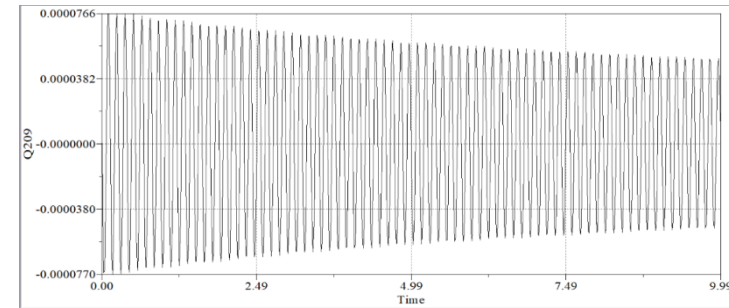


**Fig.4.47:** Deflection (m) vs Time (s) graph for Mode 2 of Concrete Slab at 400 kmph

Velocity 300 kmph

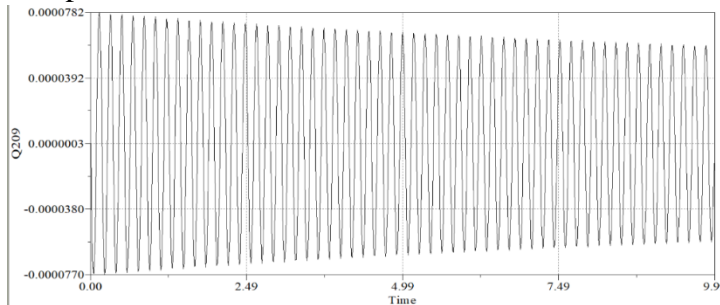


**Fig.4.46:** Deflection (m) vs Time (s) graph for Mode 2 of Concrete Slab at 300 kmph

Velocity 500 kmph

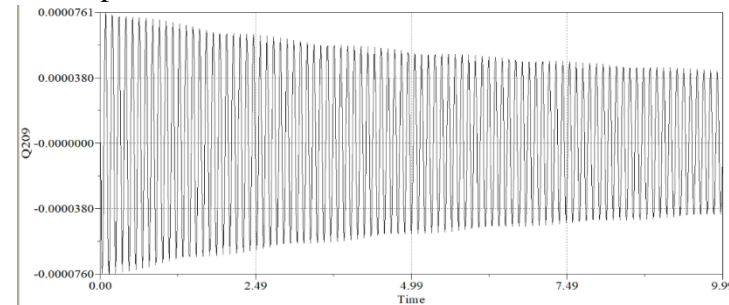


**Fig.4.48:** Deflection (m) vs Time (s) graph for Mode 2 of Concrete Slab at 500 kmph

In the above graphs it can be observed that the maximum average deflection at mode 1, for all four velocities, is 0.0771 mm, which dies out eventually, more rapidly at the velocity 500 kmph



### 4.3.3 Mode – 3

Velocity 200 kmph

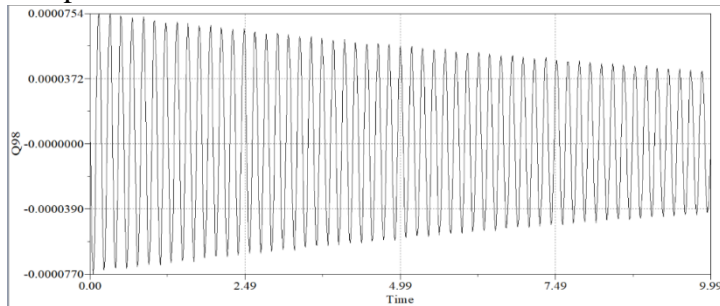


**Fig.4.49:** Deflection (m) vs Time (s) graph for Mode 3 of Concrete Slab at 200 kmph

Velocity 400 kmph

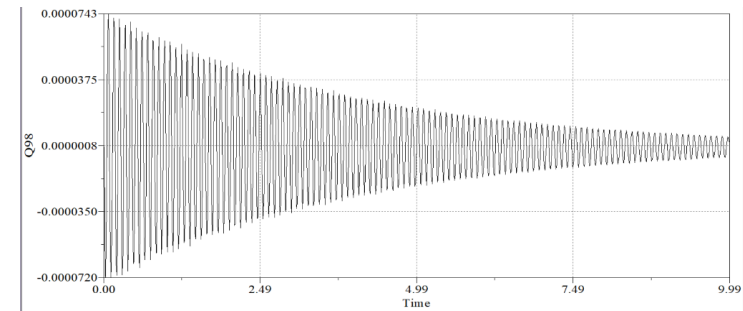


**Fig.4.51:** Deflection (m) vs Time (s) graph for Mode 3 of Concrete Slab at 400 kmph

Velocity 300 kmph

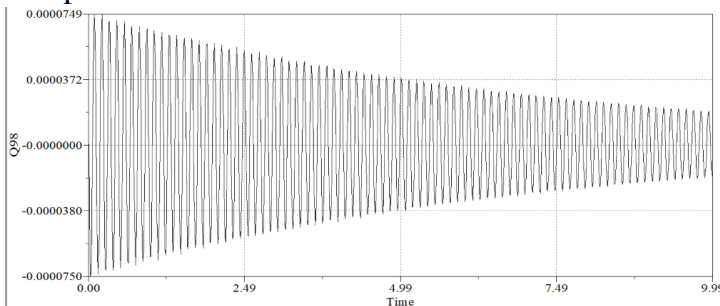


**Fig.4.50:** Deflection (m) vs Time (s) graph for Mode 3 of Concrete Slab at 300 kmph

Velocity 500 kmph

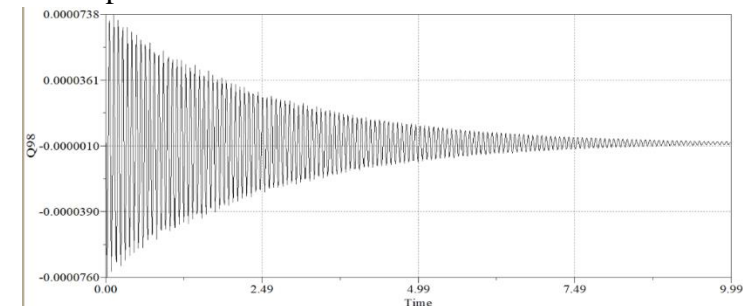


**Fig.4.52:** Deflection (m) vs Time (s) graph for Mode 3 of Concrete Slab at 500 kmph

In the above graphs it can be observed that the maximum average deflection at mode 1, for all four velocities, is 0.0748 mm, which dies out eventually, more rapidly at the velocity 500 kmph

### 4.3.4 Mode – 4

Velocity 200 kmph

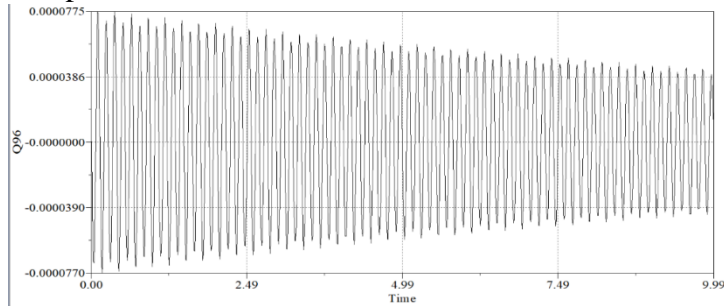


**Fig.4.53:** Deflection (m) vs Time (s) graph for Mode 4 of Concrete Slab at 200 kmph

Velocity 400 kmph

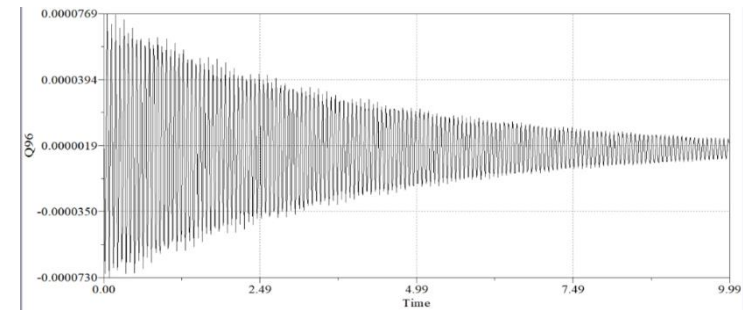


**Fig.4.55:** Deflection (m) vs Time (s) graph for Mode 4 of Concrete Slab at 400 kmph

Velocity 300 kmph

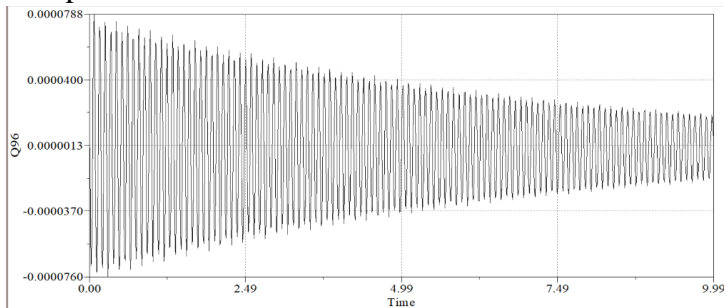


**Fig.4.54:** Deflection (m) vs Time (s) graph for Mode 4 of Concrete Slab at 300 kmph

Velocity 500 kmph

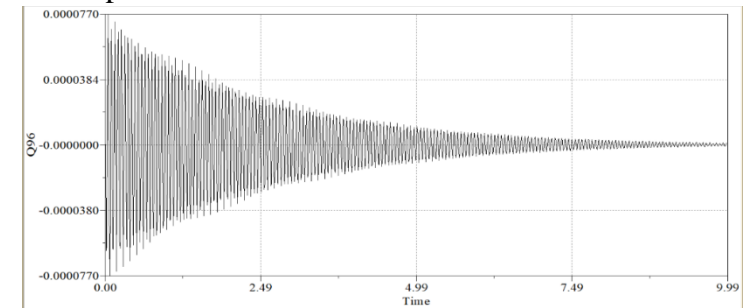


**Fig.4.56:** Deflection (m) vs Time (s) graph for Mode 4 of Concrete Slab at 500 kmph

In the above graphs it can be observed that the maximum average deflection at mode 1, for all four velocities, is 0.0766 mm , which dies out eventually, more rapidly at the velocity 500 kmph

### 4.3.5 Mode – 5

Velocity 200 kmph

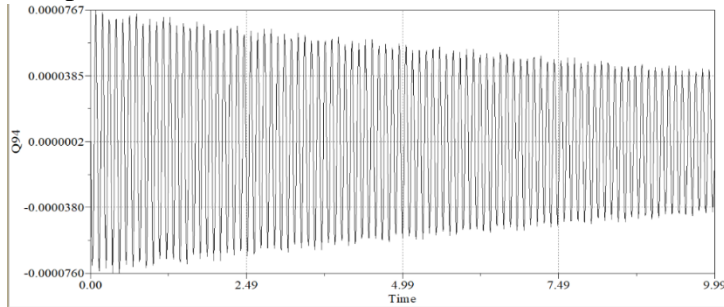


**Fig.4.57:** Deflection (m) vs Time (s) graph for Mode 5 of Concrete Slab at 200 kmph

Velocity 400 kmph

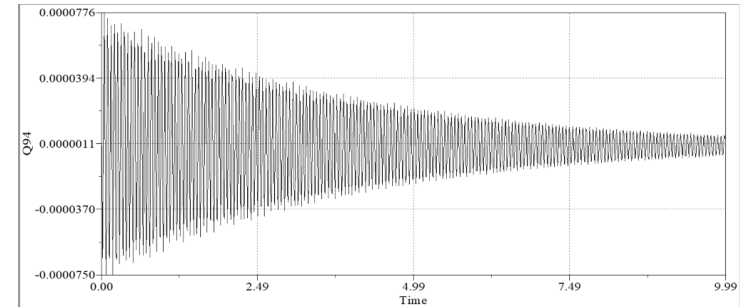


**Fig.4.59:** Deflection (m) vs Time (s) graph for Mode 5 of Concrete Slab at 400 kmph

Velocity 300 kmph

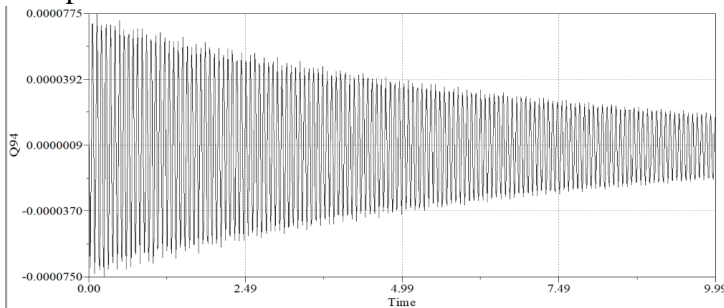


**Fig.4.58:** Deflection (m) vs Time (s) graph for Mode 5 of Concrete Slab at 300 kmph

Velocity 500 kmph

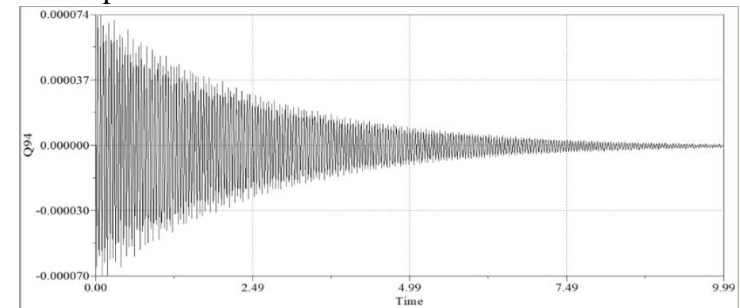


**Fig.4.60:** Deflection (m) vs Time (s) graph for Mode 5 of Concrete Slab at 500 kmph

In the above graphs it can be observed that the maximum average deflection at mode 1, for all four velocities, is 0.0752 mm, which dies out eventually, more rapidly at the velocity 500 kmph.

## 4.5 Fast Fourier Transform (FFT) for concrete slab –

### 4.5.1 Mode - 1

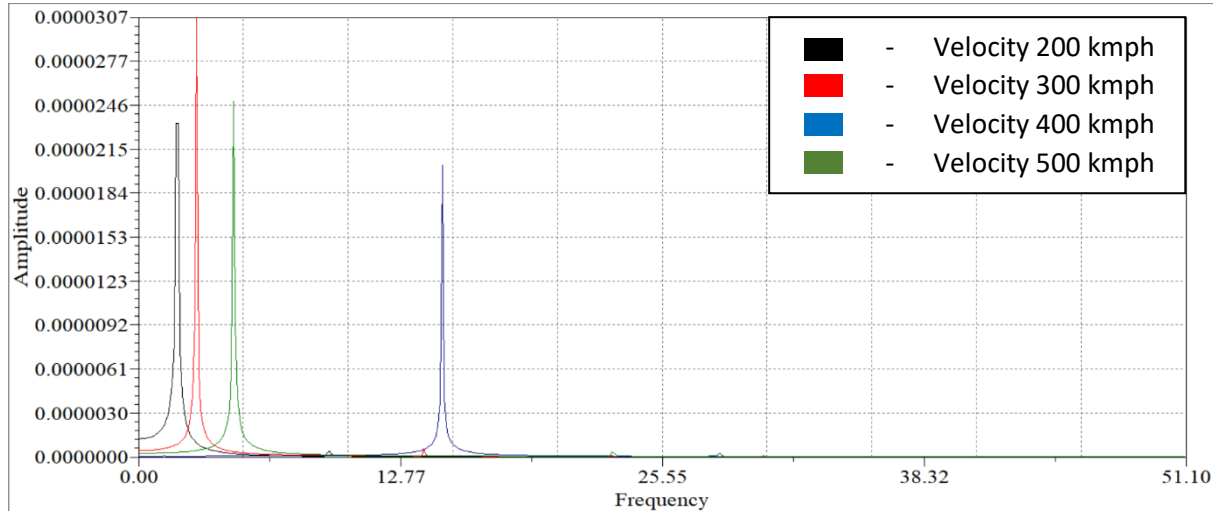


**Fig4.61:** Deflection (m) vs Frequency (Hz) Fast Fourier Transform curve of Mode 1 of Concrete Slab at different velocities

In the above graph, figure 4.61, it can be observed that the maximum value of deflection shoots up at the velocity of 300 kmph, at a frequency of about 2.5 Hz

### 4.5.2 Mode - 2

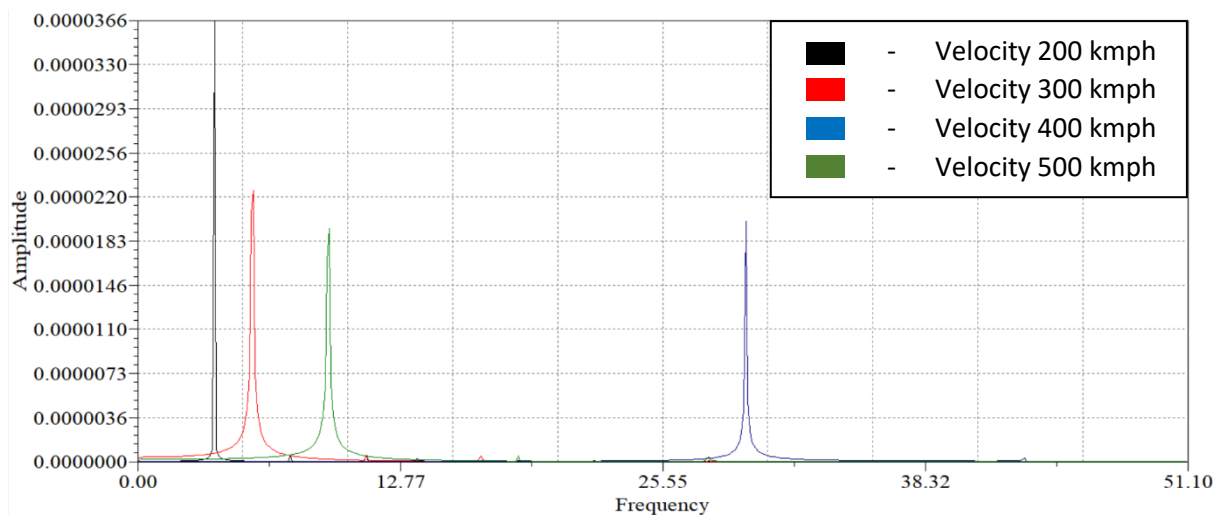


**Fig4.62:** Deflection (m) vs Frequency (Hz) Fast Fourier Transform curve of Mode 2 of Concrete Slab at different velocities

In the above graph, figure 4.62, it can be observed that the maximum value of deflection shoots up at the velocity of 200 kmph, at a frequency of about 3.5 Hz

### 4.5.3 Mode - 3

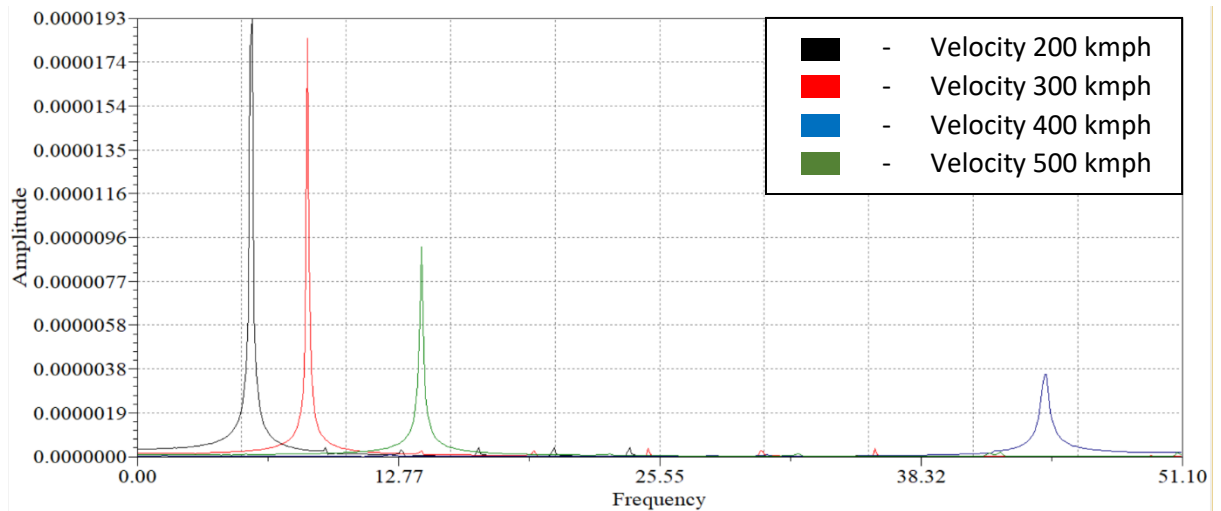


**Fig4.63:** Deflection (m) vs Frequency (Hz) Fast Fourier Transform curve of Mode 3 of Concrete Slab at different velocities

In the above graph, figure 4.63, it can be observed that the maximum value of deflection shoots up at the velocity of 200 kmph, at a frequency of about 5.5 Hz

### 4.5.4 Mode - 4

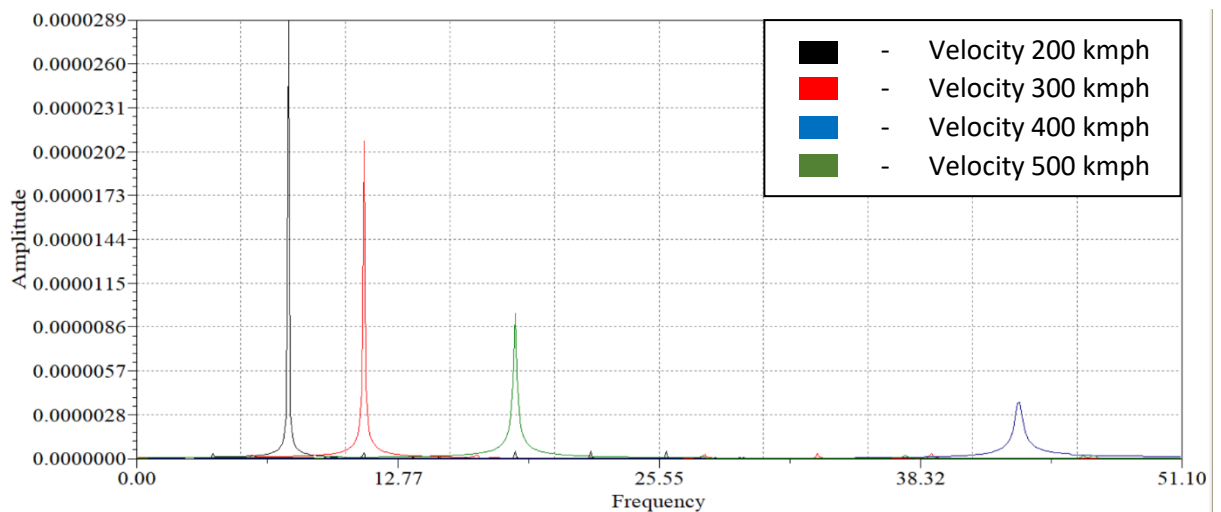


**Fig4.64:** Deflection (m) vs Frequency (Hz) Fast Fourier Transform curve of Mode 4 of Concrete Slab at different velocities

In the above graph, figure 4.64, it can be observed that the maximum value of deflection shoots up at the velocity of 200 kmph, at a frequency of about 7 Hz

#### 4.5.5 Mode – 5

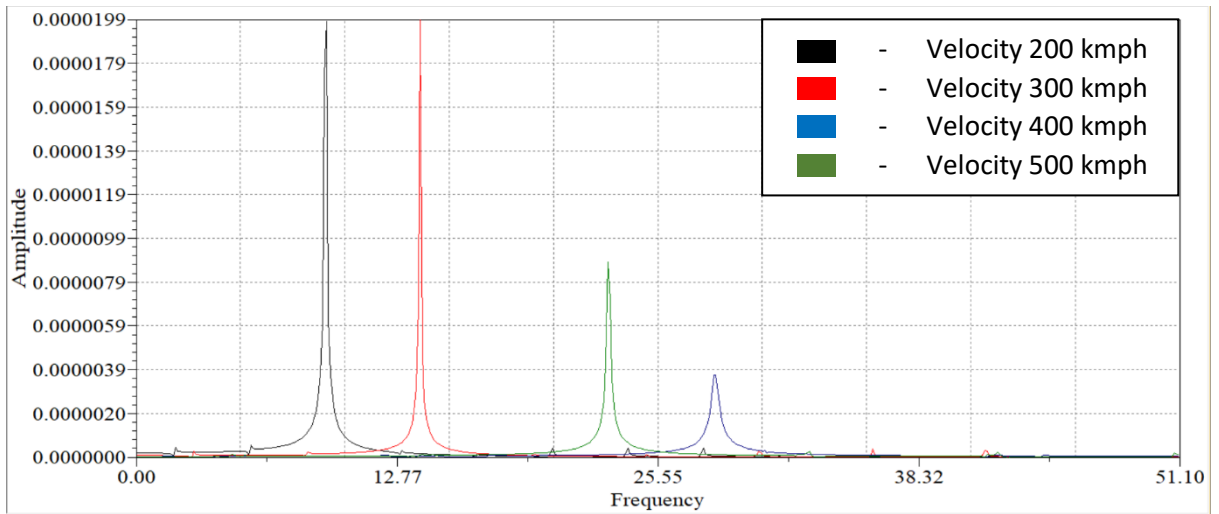


**Fig4.65:** Deflection (m) vs Frequency (Hz) Fast Fourier Transform curve of Mode 5 of Concrete Slab at different velocities

In the above graph, figure 4.65, it can be observed that the maximum value of deflection shoots up at the velocity of 200 kmph and 300 kmph, at a frequency of about 9 Hz and 13 Hz, respectively.

#### 4.5.6 Velocity 200 kmph

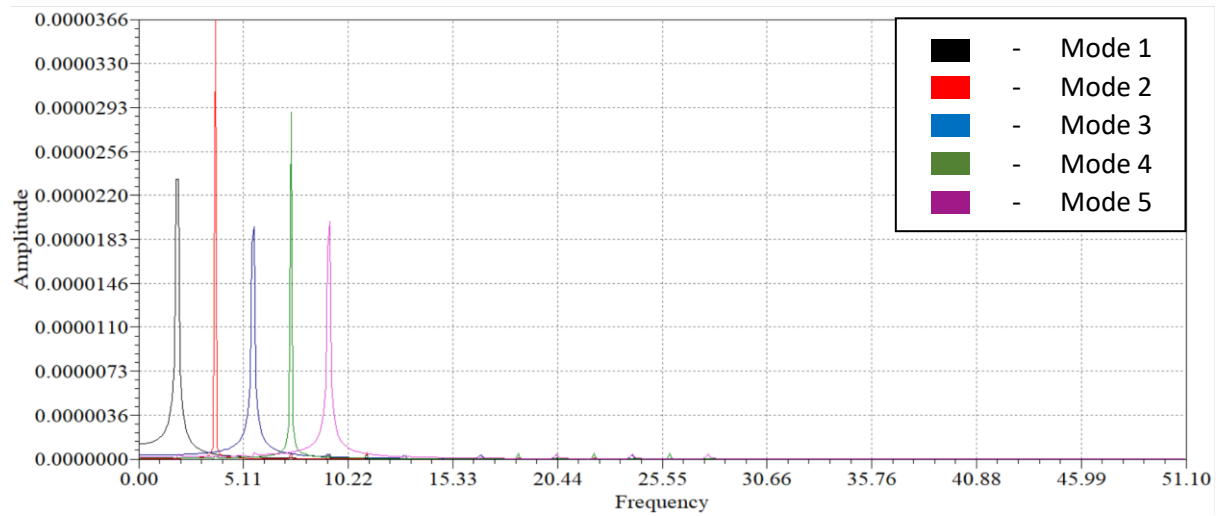


**Fig.4.66:** Deflection (m) vs Frequency (Hz) Fast Fourier Transform curve of different modes of Concrete Slab at 200 kmph velocities

#### 4.5.7 Velocity 300 kmph

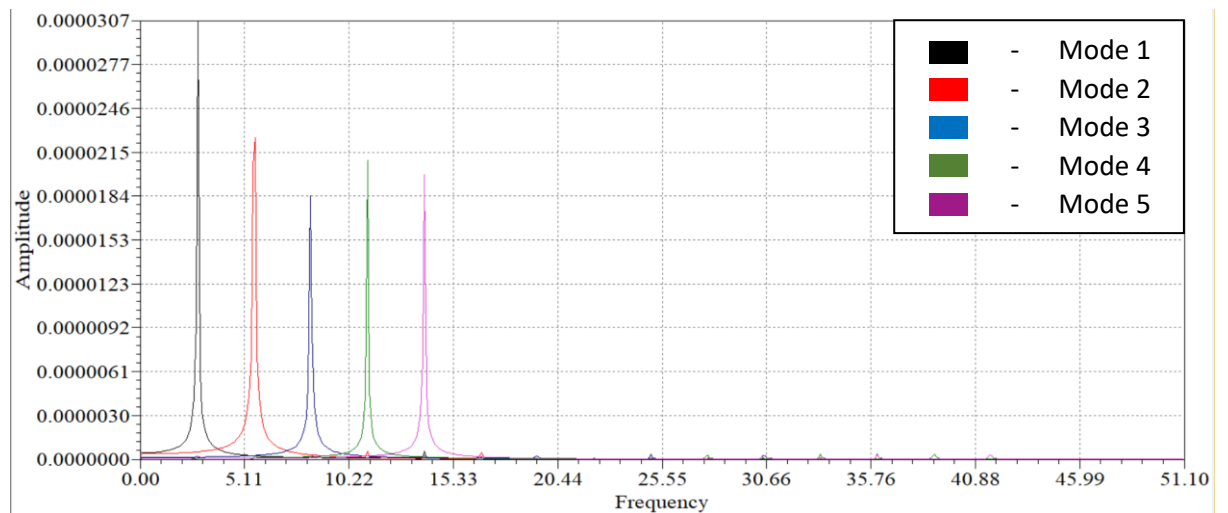


**Fig.4.67:** Deflection (m) vs Frequency (Hz) Fast Fourier Transform curve of different modes of Concrete Slab at 300 kmph velocities

#### 4.5.8 Velocity 400 kmph

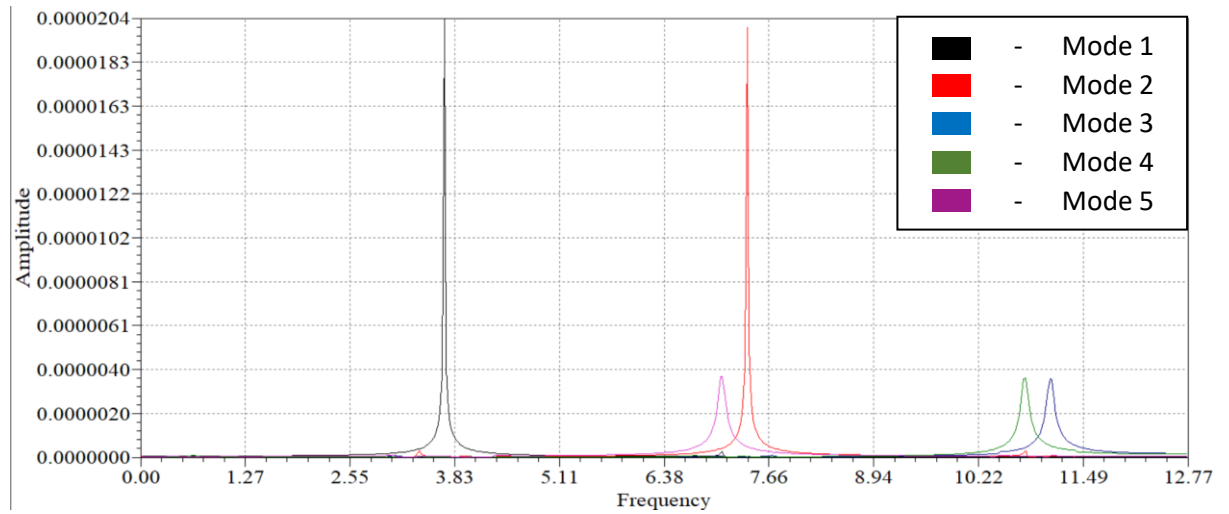


**Fig.4.68:** Deflection (m) vs Frequency (Hz) Fast Fourier Transform curve of different modes of Concrete Slab at 400 kmph velocities

#### 4.5.9 Velocity 500 kmph

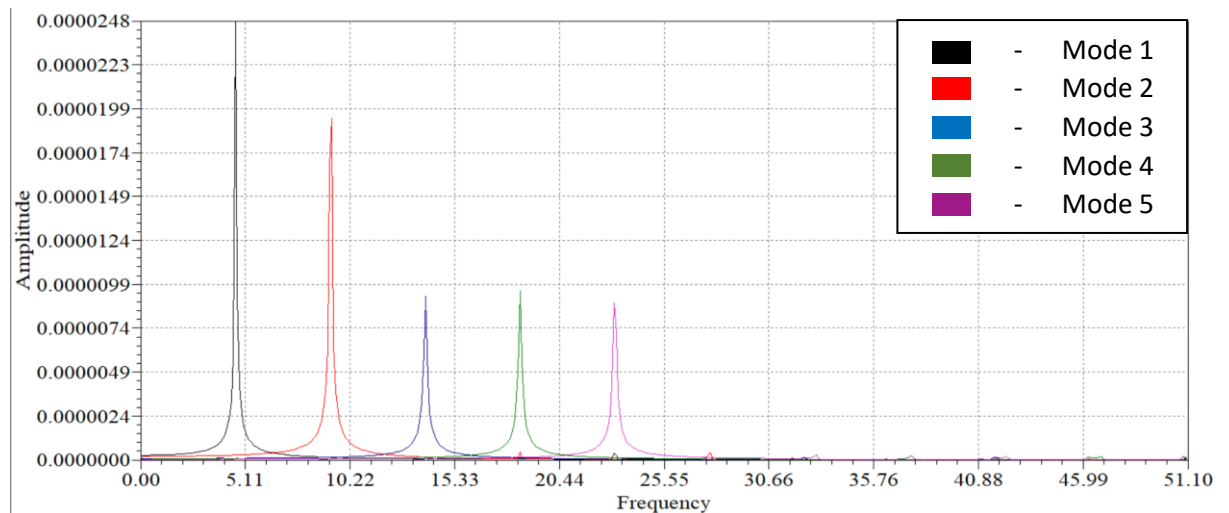


**Fig.4.69:** Deflection (m) vs Frequency (Hz) Fast Fourier Transform curve of different modes of Concrete Slab at 500 kmph velocities



In the above figures, 4.66, 4.67, 4.68, and 4.69, the Fast Fourier Transform (FFT) of mode 1, mode 2, mode 3, mode 4, and mode 5, of the concrete slab are simulated, for velocities 200 kmph, 300 kmph, 400 kmph, and 500 kmph, respectively. This is observed that for the FFT plots for various velocities, the deflection in modes 1 and 2 shoots up for irrespective of the velocities, more or less, and the deflections also follow a decreasing trend.

## **CHAPTER 5**

### **CONCLUSION AND RESULTS**

The deflection curves in the case of concrete slab, at different modes, depicts that the deflection gradually dies out as the time passes. As far as the different velocities are concerned, the trend in the graphs of the modes of concrete slab shows that, the deflection dies out with time, and with increasing velocities, the deflections die out, and reaches the value zero more rapidly. In case of concrete slab, the maximum deflection at mode 1, mode 2, mode 3, mode 4, and mode 5, at the speed of 200 kmph, 300 kmph, 400 kmph, and 500 kmph, are 0.0392 mm, 0.0387 mm, 0.0372 mm, 0.0381 mm, and 0.0376 mm, respectively.

The Fast Fourier Transform (FFT) of the concrete slab, at different modes, for different velocities, depicts that the excitation of Mode 1 is highest at the speed of 300 kmph, at a value of 0.0307 mm. The excitation of Mode 2 is highest at the speed of 200 kmph, at a value of approximately 0.0366 mm. The excitation of Mode 3 is highest at the speed of 200 kmph, at a value of 0.0193 mm, closely followed by 300 kmph speed, at a value of 0.0183 mm. The excitation of Mode 4 is also highest at the speed of 200 kmph, at a value of 0.0289 mm. And the excitation of Mode 5 is highest at the speed of 200 and 300 kmph, both, at a value of 0.0199 mm. This observation hints that the maximum deflection occurs around the velocity of 200 kmph and in mode 2.

The present study deals with a two-layer problem of beam modelling, in three-dimensions, for a concrete slab – sub grade system. In the future the same methods can be extended for multi-layer bond graph modelling in three-dimensions. A more complex system, involving the vehicle as well, on the multi-layered track, can be performed, using bond graph capsules and ports.

## REFERENCES

- [1] Karmakar, R. and Mukherjee, A., 1990. Dynamics of electric overhead travelling cranes: A bond graph approach. *Mechanism and Machine Theory*, 25(1), pp.29-39.
- [2] Knothe, K.L. and Grassie, S.L., 1993. Modelling of railway track and vehicle/track interaction at high frequencies. *Vehicle system dynamics*, 22(3-4), pp.209-262.
- [3] Zeng, J. and Dai, H., 1994. The Dynamic Simulation Of Vehicle–Bridge Interactions Using Bond Graph Technique. *Vehicle System Dynamics*, 23(S1), pp.591-602.
- [4] Nielsen, J.C. and Igeland, A., 1995. Vertical dynamic interaction between train and track influence of wheel and track imperfections. *Journal of sound and vibration*, 187(5), pp.825-839.
- [5] Broenink, J.F., 1999. Introduction to physical systems modelling with bond graphs. *SiE Whitebook on Simulation Methodologies*, 31.
- [6] Chan, C.C., 2002. The state of the art of electric and hybrid vehicles. *Proceedings of the IEEE*, 90(2), pp.247-275.
- [7] Kumaran, G., Menon, D. and Nair, K.K., 2002. Dynamic response of railtrack sleepers to moving train loads. *Proceedings of EURO-DYN-02, Swets & Zeitlinger, Lisse*, pp.1185-1190.
- [8] Bureika, G. and Subačius, R., 2002. Mathematical model of dynamic interaction between wheel-set and rail track. *Transport*, 17(2), pp.46-51.
- [9] Samantaray, A., 2003. About Bond Graph–The system modeling world. *Available online via <http://www.bondgraphs.com/about.html> [Accessed April 6 2003]*.
- [10] Kumaxl, H. and Sujatha, B.S.K.C., 2005. Lateral dynamic analysis of a typical Indian rail-road vehicle.
- [11] Uzzal, R. U. A., Ahmed, W., and Rakheja, S. (2008). Dynamic analysis of railway vehicle-track interactions due to wheel flat with a pitch-plane vehicle model. *Journal of Mechanical Engineering*, 39(2), 86-94.

- [12] Kumar, V. and Rastogi, V., 2009. Investigation of vertical dynamic behaviour and modelling of a typical Indian rail road vehicle through bond graph. *World Journal of Modelling and Simulation*, 5(2), pp.130-138.
- [13] Gustafsson, A., 2009. Reduced models for dynamic analysis of high-speed railway bridges.
- [14] Kumar, V. and Rastogi, V., 2009. Lateral Dynamic Analysis of Rail Road Vehicle through Bond Graph Modeling.
- [15] Nguyen Gia, K., Goicolea Ruigómez, J.M. and Gabaldón Castillo, F., 2010. Dynamic Analysis of High Speed Railway Traffic Loads on Ballasted Track.
- [16] Nguyen, K., Goicolea, J.M., Nguyen, K., and Galbadon, F., 2011, October. Dynamic Analysis of High Speed Railway Traffic Loads on Ballasted Track. In *Advances in Environmental Vibration, Fifth International Symposium on Environmental Vibration, Chengdu, China*.
- [17] Lei, X., Wu, S. and Zhang, B., 2016. Dynamic analysis of the high speed train and slab track nonlinear coupling system with the cross iteration algorithm. *Journal of Nonlinear Dynamics*, 2016.
- [18] Cao, T.N.T., Reddy, J.N., Ang, K.K., Luong, V.H., Tran, M.T. and Dai, J., 2018. Dynamic analysis of three-dimensional high-speed train-track model using moving element method. *Advances in Structural Engineering*, 21(6), pp.862-876.
- [19] Kumar, V., 2018. Investigation of structural dynamics and ride comfort of rail vehicle system.
- [20] Kumar, V., Rastogi, V. and Pathak, P.M., 2018. Effect of Non-linearity on Wheel/rail Interaction Dynamics using Bond Graph.

## APPENDIX

Equations generated from the model

$$\begin{aligned}
 dY[0]= & z1*(K78*Y[31]+R79*(z5*Y[5]/M102+z4*Y[6]/M56+z3*Y[4]/M103-z2*Y[1]/M181 \\
 & -z1*Y[0]/M190))+z1*(K82*Y[30]+R83*(z5*Y[5]/M102+z4*Y[6]/M56+z3*Y[4]/M103 \\
 & -z2*Y[1]/M181-z1*Y[0]/M190))+z1*(K75*Y[32]+R76*(z5*Y[5]/M102+z4*Y[6]/M56 \\
 & +z3*Y[4]/M103-z2*Y[1]/M181-z1*Y[0]/M190))-z1*(K204*Y[13] \\
 & +R205*(z2*Y[1]/M181+z1*Y[0]/M190+z3*Y[4]/M103+z4*Y[6]/M56+z5*Y[5]/M102)) \\
 & -z1*(K206*Y[12]+R207*(z1*Y[0]/M190+z2*Y[1]/M181+z3*Y[4]/M103+z4*Y[6]/M56 \\
 & +z5*Y[5]/M102))+z1*SE137-K189*Y[15]+K212*Y[11]+R213*(-Y[2]/M154- \\
 & Y[0]/M190);
 \end{aligned}$$

$$\begin{aligned}
 dY[1]= & z2*(K78*Y[31]+R79*(z5*Y[5]/M102+z4*Y[6]/M56+z3*Y[4]/M103-z2*Y[1]/M181 \\
 & -z1*Y[0]/M190))+z2*(K82*Y[30]+R83*(z5*Y[5]/M102+z4*Y[6]/M56+z3*Y[4]/M103 \\
 & -z2*Y[1]/M181-z1*Y[0]/M190))+z2*(K75*Y[32]+R76*(z5*Y[5]/M102+z4*Y[6]/M56 \\
 & +z3*Y[4]/M103-z2*Y[1]/M181-z1*Y[0]/M190))-z2*(K204*Y[13] \\
 & +R205*(z2*Y[1]/M181+z1*Y[0]/M190+z3*Y[4]/M103+z4*Y[6]/M56+z5*Y[5]/M102)) \\
 & -z2*(K206*Y[12]+R207*(z1*Y[0]/M190+z2*Y[1]/M181+z3*Y[4]/M103+z4*Y[6]/M56 \\
 & +z5*Y[5]/M102))+z2*SE137-K180*Y[14]+K209*Y[10]+R210*(-Y[3]/M145- \\
 & Y[1]/M181);
 \end{aligned}$$

$$\begin{aligned}
 dY[2]= & z1*(K28*Y[36]+R29*(z3*Y[9]/M4+z4*Y[8]/M9+z5*Y[7]/M14-z1*Y[2]/M154 \\
 & -z2*Y[3]/M145))+z1*(K35*Y[34]+R36*(z3*Y[9]/M4+z4*Y[8]/M9+z5*Y[7]/M14 \\
 & -z2*Y[3]/M145-z1*Y[2]/M154))+z1*(K31*Y[35]+R32*(z3*Y[9]/M4+z4*Y[8]/M9
 \end{aligned}$$

$$\begin{aligned}
& +z5*Y[7]/M14-z2*Y[3]/M145-z1*Y[2]/M154))-z1*(K164*Y[18]+R165*(z2*Y[3]/M145 \\
& +z1*Y[2]/M154+z3*Y[9]/M4+z4*Y[8]/M9+z5*Y[7]/M14))-K153*Y[16] \\
& -z1*(K172*Y[17]+R173*(z1*Y[2]/M154+z2*Y[3]/M145+z3*Y[9]/M4+z4*Y[8]/M9 \\
& +z5*Y[7]/M14))+z1*SE122+K212*Y[11]+R213*(-Y[2]/M154-Y[0]/M190); \\
dY[3]= & z2*(K28*Y[36]+R29*(z3*Y[9]/M4+z4*Y[8]/M9+z5*Y[7]/M14-z1*Y[2]/M154 \\
& -z2*Y[3]/M145))+z2*(K35*Y[34]+R36*(z3*Y[9]/M4+z4*Y[8]/M9+z5*Y[7]/M14 \\
& -z2*Y[3]/M145-z1*Y[2]/M154))+z2*(K31*Y[35]+R32*(z3*Y[9]/M4+z4*Y[8]/M9 \\
& +z5*Y[7]/M14-z2*Y[3]/M145-z1*Y[2]/M154))-z2*(K164*Y[18]+R165*(z2*Y[3]/M145 \\
& +z1*Y[2]/M154+z3*Y[9]/M4+z4*Y[8]/M9+z5*Y[7]/M14))-K144*Y[19] \\
& -z2*(K172*Y[17]+R173*(z1*Y[2]/M154+z2*Y[3]/M145+z3*Y[9]/M4+z4*Y[8]/M9 \\
& +z5*Y[7]/M14))+z2*SE122+K209*Y[10]+R210*(-Y[3]/M145-Y[1]/M181); \\
dY[4]= & -z3*(K75*Y[32]+R76*(z5*Y[5]/M102+z4*Y[6]/M56+z3*Y[4]/M103-z2*Y[1]/M181 \\
& -z1*Y[0]/M190))-z3*(K82*Y[30]+R83*(z5*Y[5]/M102+z4*Y[6]/M56+z3*Y[4]/M103 \\
& -z2*Y[1]/M181-z1*Y[0]/M190))-z3*(K78*Y[31]+R79*(z5*Y[5]/M102+z4*Y[6]/M56 \\
& +z3*Y[4]/M103-z2*Y[1]/M181-z1*Y[0]/M190))-z3*SE137-K98*Y[26]-R99*(Y[9]/M4 \\
& +Y[4]/M103)-K109*Y[20]-z3*(K204*Y[13]+R205*(z2*Y[1]/M181+z1*Y[0]/M190 \\
& +z3*Y[4]/M103+z4*Y[6]/M56+z5*Y[5]/M102))- \\
& z3*(K206*Y[12]+R207*(z1*Y[0]/M190 \\
& +z2*Y[1]/M181+z3*Y[4]/M103+z4*Y[6]/M56+z5*Y[5]/M102)); \\
dY[5]= & -z5*(K75*Y[32]+R76*(z5*Y[5]/M102+z4*Y[6]/M56+z3*Y[4]/M103-z2*Y[1]/M181 \\
& -z1*Y[0]/M190))-z5*(K82*Y[30]+R83*(z5*Y[5]/M102+z4*Y[6]/M56+z3*Y[4]/M103 \\
& -z2*Y[1]/M181-z1*Y[0]/M190))-z5*(K78*Y[31]+R79*(z5*Y[5]/M102+z4*Y[6]/M56
\end{aligned}$$

$$\begin{aligned}
& +z^3*Y[4]/M103-z^2*Y[1]/M181-z^1*Y[0]/M190))-z^5*SE137-K94*Y[28]-R95*(Y[7]/M14 \\
& +Y[5]/M102)-K107*Y[22]-z^5*(K204*Y[13]+R205*(z^2*Y[1]/M181+z^1*Y[0]/M190 \\
& +z^3*Y[4]/M103+z^4*Y[6]/M56+z^5*Y[5]/M102))- \\
& z^5*(K206*Y[12]+R207*(z^1*Y[0]/M190 \\
& +z^2*Y[1]/M181+z^3*Y[4]/M103+z^4*Y[6]/M56+z^5*Y[5]/M102));
\end{aligned}$$

$$\begin{aligned}
dY[6]=& -z^4*(K75*Y[32]+R76*(z^5*Y[5]/M102+z^4*Y[6]/M56+z^3*Y[4]/M103-z^2*Y[1]/M181 \\
& -z^1*Y[0]/M190))-z^4*(K82*Y[30]+R83*(z^5*Y[5]/M102+z^4*Y[6]/M56+z^3*Y[4]/M103 \\
& -z^2*Y[1]/M181-z^1*Y[0]/M190))-z^4*(K78*Y[31]+R79*(z^5*Y[5]/M102+z^4*Y[6]/M56 \\
& +z^3*Y[4]/M103-z^2*Y[1]/M181-z^1*Y[0]/M190))-z^4*SE137-K96*Y[27]-R97*(Y[8]/M9 \\
& +Y[6]/M56)-K108*Y[21]-z^4*(K204*Y[13]+R205*(z^2*Y[1]/M181+z^1*Y[0]/M190 \\
& +z^3*Y[4]/M103+z^4*Y[6]/M56+z^5*Y[5]/M102))- \\
& z^4*(K206*Y[12]+R207*(z^1*Y[0]/M190 \\
& +z^2*Y[1]/M181+z^3*Y[4]/M103+z^4*Y[6]/M56+z^5*Y[5]/M102));
\end{aligned}$$

$$\begin{aligned}
dY[7]=& -z^5*(K28*Y[36]+R29*(z^3*Y[9]/M4+z^4*Y[8]/M9+z^5*Y[7]/M14-z^1*Y[2]/M154 \\
& -z^2*Y[3]/M145))-z^5*(K35*Y[34]+R36*(z^3*Y[9]/M4+z^4*Y[8]/M9+z^5*Y[7]/M14 \\
& -z^2*Y[3]/M145-z^1*Y[2]/M154))-z^5*(K31*Y[35]+R32*(z^3*Y[9]/M4+z^4*Y[8]/M9 \\
& +z^5*Y[7]/M14-z^2*Y[3]/M145-z^1*Y[2]/M154))-z^5*SE122-K94*Y[28]-R95*(Y[7]/M14 \\
& +Y[5]/M102)-K106*Y[23]-z^5*(K164*Y[18]+R165*(z^2*Y[3]/M145+z^1*Y[2]/M154 \\
& +z^3*Y[9]/M4+z^4*Y[8]/M9+z^5*Y[7]/M14))-z^5*(K172*Y[17]+R173*(z^1*Y[2]/M154 \\
& +z^2*Y[3]/M145+z^3*Y[9]/M4+z^4*Y[8]/M9+z^5*Y[7]/M14));
\end{aligned}$$

$$\begin{aligned}
dY[8]=& -z^4*(K28*Y[36]+R29*(z^3*Y[9]/M4+z^4*Y[8]/M9+z^5*Y[7]/M14-z^1*Y[2]/M154 \\
& -z^2*Y[3]/M145))-z^4*(K35*Y[34]+R36*(z^3*Y[9]/M4+z^4*Y[8]/M9+z^5*Y[7]/M14
\end{aligned}$$

$$\begin{aligned}
& -z^2*Y[3]/M145-z^1*Y[2]/M154))-z^4*(K31*Y[35]+R32*(z^3*Y[9]/M4+z^4*Y[8]/M9 \\
& +z^5*Y[7]/M14-z^2*Y[3]/M145-z^1*Y[2]/M154))-z^4*SE122-K96*Y[27]-R97*(Y[8]/M9 \\
& +Y[6]/M56)-K105*Y[24]-z^4*(K164*Y[18]+R165*(z^2*Y[3]/M145+z^1*Y[2]/M154 \\
& +z^3*Y[9]/M4+z^4*Y[8]/M9+z^5*Y[7]/M14))-z^4*(K172*Y[17]+R173*(z^1*Y[2]/M154 \\
& +z^2*Y[3]/M145+z^3*Y[9]/M4+z^4*Y[8]/M9+z^5*Y[7]/M14));
\end{aligned}$$

$$\begin{aligned}
dY[9]=& -z^3*(K28*Y[36]+R29*(z^3*Y[9]/M4+z^4*Y[8]/M9+z^5*Y[7]/M14-z^1*Y[2]/M154 \\
& -z^2*Y[3]/M145))-z^3*(K35*Y[34]+R36*(z^3*Y[9]/M4+z^4*Y[8]/M9+z^5*Y[7]/M14 \\
& -z^2*Y[3]/M145-z^1*Y[2]/M154))-z^3*(K31*Y[35]+R32*(z^3*Y[9]/M4+z^4*Y[8]/M9 \\
& +z^5*Y[7]/M14-z^2*Y[3]/M145-z^1*Y[2]/M154))-z^3*SE122-K98*Y[26]-R99*(Y[9]/M4 \\
& +Y[4]/M103)-K104*Y[25]-z^3*(K164*Y[18]+R165*(z^2*Y[3]/M145+z^1*Y[2]/M154 \\
& +z^3*Y[9]/M4+z^4*Y[8]/M9+z^5*Y[7]/M14))-z^3*(K172*Y[17]+R173*(z^1*Y[2]/M154 \\
& +z^2*Y[3]/M145+z^3*Y[9]/M4+z^4*Y[8]/M9+z^5*Y[7]/M14));
\end{aligned}$$

$$dY[10]=-Y[3]/M145-Y[1]/M181;$$

$$dY[11]=-Y[2]/M154-Y[0]/M190;$$

$$dY[12]=z^1*Y[0]/M190+z^2*Y[1]/M181+z^3*Y[4]/M103+z^4*Y[6]/M56+z^5*Y[5]/M102;$$

$$dY[13]=z^2*Y[1]/M181+z^1*Y[0]/M190+z^3*Y[4]/M103+z^4*Y[6]/M56+z^5*Y[5]/M102;$$

$$dY[14]=Y[1]/M181;$$

$$dY[15]=Y[0]/M190;$$

$$dY[16]=Y[2]/M154;$$

$$dY[17]=z^1*Y[2]/M154+z^2*Y[3]/M145+z^3*Y[9]/M4+z^4*Y[8]/M9+z^5*Y[7]/M14;$$

$$dY[18]=z^2*Y[3]/M145+z^1*Y[2]/M154+z^3*Y[9]/M4+z^4*Y[8]/M9+z^5*Y[7]/M14;$$



$$dY[19]=Y[3]/M145;$$

$$dY[20]=Y[4]/M103;$$

$$dY[21]=Y[6]/M56;$$

$$dY[22]=Y[5]/M102;$$

$$dY[23]=Y[7]/M14;$$

$$dY[24]=Y[8]/M9;$$

$$dY[25]=Y[9]/M4;$$

$$dY[26]=Y[9]/M4+Y[4]/M103;$$

$$dY[27]=Y[8]/M9+Y[6]/M56;$$

$$dY[28]=Y[7]/M14+Y[5]/M102;$$

$$dY[29]=1/R90*(SE137-K89*Y[29]);$$

$$dY[30]=z5*Y[5]/M102+z4*Y[6]/M56+z3*Y[4]/M103-z2*Y[1]/M181-z1*Y[0]/M190;$$

$$dY[31]=z5*Y[5]/M102+z4*Y[6]/M56+z3*Y[4]/M103-z2*Y[1]/M181-z1*Y[0]/M190;$$

$$dY[32]=z5*Y[5]/M102+z4*Y[6]/M56+z3*Y[4]/M103-z2*Y[1]/M181-z1*Y[0]/M190;$$






































$$dY[33]=1/R43*(SE122-K42*Y[33]);$$

$$dY[34]=z3*Y[9]/M4+z4*Y[8]/M9+z5*Y[7]/M14-z2*Y[3]/M145-z1*Y[2]/M154;$$

$$dY[35]=z3*Y[9]/M4+z4*Y[8]/M9+z5*Y[7]/M14-z2*Y[3]/M145-z1*Y[2]/M154;$$

$$dY[36]=z3*Y[9]/M4+z4*Y[8]/M9+z5*Y[7]/M14-z1*Y[2]/M154-z2*Y[3]/M145;$$

Expressions used in the model:

Variable	Assignment
 C_sub (double)	
 K28 (double)	K28=C_sub;
 R_sub (double)	
 R29 (double)	R29=R_sub;
 K31 (double)	K31=C_sub;
 R32 (double)	R32=R_sub;
 K35 (double)	K35=C_sub;
 R36 (double)	R36=R_sub;
 rho (double)	
 L (double)	
 A (double)	
 Mv (double)	$Mv = (\rho * L * A) / 4;$
 M4 (double)	M4=Mv;
 M9 (double)	M9=Mv;
 M14 (double)	M14=Mv;
 C_contact	
 K42 (double)	K42=C_contact;
 R_contact	
 R43 (double)	R43=R_contact;
 K75 (double)	K75=C_sub;
 R76 (double)	R76=R_sub;
 K78 (double)	K78=C_sub;
 R79 (double)	R79=R_sub;
 K82 (double)	K82=C_sub;
 R83 (double)	R83=R_sub;
 M56 (double)	M56=Mv;
 K89 (double)	K89=C_contact;
 R90 (double)	R90=R_contact;
 C_lat (double)	
 K94 (double)	K94=C_lat;
 R_lat (double)	
 R95 (double)	R95=R_lat;
 K96 (double)	K96=C_lat;
 R97 (double)	R97=R_lat;
 K98 (double)	K98=C_lat;
 R99 (double)	R99=R_lat;
 M102 (double)	M102=Mv;

Variable	Assignment
M103 (double)	M103=Mv;
PI (double)	PI=3.14;
v (double)	
x (double)	x=v*t;
z1 (double)	z1=sin((PI*x)/L);
z2 (double)	z2=sin((2*PI*x)/L);
z3 (double)	z3=sin((3*PI*x)/L);
EI (double)	
omega1 (double)	omega1=(PI/L)*(PI/L)*(sqrt(EI/rho*A));
C1_slab (double)	C1_slab=Mv*omega1*omega1;
omega3 (double)	omega3=(3*PI/L)*(3*PI/L)*(sqrt(EI/rho*A));
C3_slab (double)	C3_slab=Mv*omega3*omega3;
K104 (double)	K104=C3_slab;
omega2 (double)	omega2=(2*PI/L)*(2*PI/L)*(sqrt(EI/rho*A));
C2_slab (double)	C2_slab=Mv*omega2*omega2;
omega4 (double)	omega4=(4*PI/L)*(4*PI/L)*(sqrt(EI/rho*A));
C4_slab (double)	C4_slab=Mv*omega4*omega4;
K105 (double)	K105=C4_slab;
omega5 (double)	omega5=(5*PI/L)*(5*PI/L)*(sqrt(EI/rho*A));
C5_slab (double)	C5_slab=Mv*omega5*omega5;
K106 (double)	K106=C5_slab;
K107 (double)	K107=C5_slab;
K108 (double)	K108=C4_slab;
K109 (double)	K109=C3_slab;
z4 (double)	z4=sin((4*PI*x)/L);
z5 (double)	z5=sin((5*PI*x)/L);
load (double)	
SE137 (double)	SE137=load;
SE122 (double)	SE122=load;
M145 (double)	M145=Mv;
K144 (double)	K144=C2_slab;
K164 (double)	K164=C_sub;
R165 (double)	R165=R_sub;
K172 (double)	K172=C_sub;
R173 (double)	R173=R_sub;
M154 (double)	M154=Mv;
K153 (double)	K153=C1_slab;

Variable	Assignment
$\rho$ (double)	$\rho = \rho$
omega2 (double)	$\omega_2 = (2 \cdot \pi / L) \cdot (2 \cdot \pi / L) \cdot (\sqrt{EI / \rho \cdot A})$
C2_slab (double)	$C2\_slab = Mv \cdot \omega_2 \cdot \omega_2$
omega4 (double)	$\omega_4 = (4 \cdot \pi / L) \cdot (4 \cdot \pi / L) \cdot (\sqrt{EI / \rho \cdot A})$
C4_slab (double)	$C4\_slab = Mv \cdot \omega_4 \cdot \omega_4$
K105 (double)	$K105 = C4\_slab$
omega5 (double)	$\omega_5 = (5 \cdot \pi / L) \cdot (5 \cdot \pi / L) \cdot (\sqrt{EI / \rho \cdot A})$
C5_slab (double)	$C5\_slab = Mv \cdot \omega_5 \cdot \omega_5$
K106 (double)	$K106 = C5\_slab$
K107 (double)	$K107 = C5\_slab$
K108 (double)	$K108 = C4\_slab$
K109 (double)	$K109 = C3\_slab$
z4 (double)	$z_4 = \sin((4 \cdot \pi \cdot x) / L)$
z5 (double)	$z_5 = \sin((5 \cdot \pi \cdot x) / L)$
load (double)	
SE137 (double)	$SE137 = load$
SE122 (double)	$SE122 = load$
M145 (double)	$M145 = Mv$
K144 (double)	$K144 = C2\_slab$
K164 (double)	$K164 = C\_sub$
R165 (double)	$R165 = R\_sub$
K172 (double)	$K172 = C\_sub$
R173 (double)	$R173 = R\_sub$
M154 (double)	$M154 = Mv$
K153 (double)	$K153 = C1\_slab$
M181 (double)	$M181 = Mv$
M190 (double)	$M190 = Mv$
K189 (double)	$K189 = C1\_slab$
K180 (double)	$K180 = C2\_slab$
K204 (double)	$K204 = C\_sub$
K206 (double)	$K206 = C\_sub$
R205 (double)	$R205 = R\_sub$
R207 (double)	$R207 = R\_sub$
K212 (double)	$K212 = C\_lat$
K209 (double)	$K209 = C\_lat$
R210 (double)	$R210 = R\_lat$
R213 (double)	$R213 = R\_lat$